



Groundwater geochemical evolution, origin and quality in the Lower Pra Basin, Ghana: Insights from hydrogeochemistry, multivariate statistical analysis, mineral saturation indices, stable isotopes ($\delta^2\text{H}$ and $\delta^{18}\text{O}$) and geostatistical analysis

Samuel Y. Ganyaglo^{1,2} · Joel Y. Binyiako¹ · Emmanuel M. Teye³ · Abass Gibrilla² · Dickson Abdul-Wahab¹ · Samuel Edusei⁴ · Paulina Amponsah¹ · Courage D. Egbi² · Samuel B. Dampare¹ · Ebenezer Aquisman Asare²

Received: 27 May 2024 / Revised: 12 July 2024 / Accepted: 23 July 2024

© The Author(s), under exclusive licence to Science Press and Institute of Geochemistry, CAS and Springer-Verlag GmbH Germany, part of Springer Nature 2024

Abstract In many places across the globe, including the Wassa District of Ghana, groundwater provides a significant supply of water for various purposes. Understanding the groundwater origin and hydrogeochemical processes controlling the groundwater chemistry is a major step in the sustainable management of the aquifers. A total of 29 groundwater samples were collected and analysed. Ionic ratio graphs, multivariate statistical analysis, mineral saturation indices, stable isotopes, and geostatistics methods were used to examine the sources and the quality of the groundwater. The findings describe the water types in the district as Ca–Mg–HCO₃–Cl, Ca–Na–HCO₃, Na–Ca–HCO₃, Ca–Na–HCO₃–Cl, Na–Ca–HCO₃–Cl, mix water type, Na–HCO₃–Cl, with possible evolution to Ca–Na–Cl–HCO₃, and Na–Ca–Cl–HCO₃. According to the IEWQI for drinking water, around 53.6% of the samples have good quality, whereas 10.7% have very low-quality groundwater. Only 3.45% of the samples are suitable to use for irrigation without treatment, whereas 41.4% are somewhat safe with minimal treatment. Water-rock interactions, including the dissolution and weathering of silicate minerals, cation exchange processes, and human activities like mining and

quarrying, are some of the main factors influencing groundwater chemistry. Principal component analysis revealed that groundwater chemistry is influenced by a combination of natural and anthropogenic sources. The APCs-MLR receptor model quantifies the factors that play important roles in groundwater salinization, including mineral dissolution and weathering (19.4%), localised Cd (16%), Ni (14.6%), Pb (12.8%), and Fe (11.4%) contamination from urbanisation while unidentified sources of pollution account for about 26.0%. The stable isotopes revealed groundwater is of meteoric origin and water-rock interaction the major mechanism for groundwater mineralization. The results of this research highlight the need of implementing an integrated strategy for managing and accessing groundwater quality.

Keywords Groundwater · Integrated approaches · Stable isotopes · Hydrochemical facies · Water-rock interaction · Quality assessment · Empirical Bayesian kriging

1 Introduction

The global demand for groundwater has increased exponentially as it continues to be an extremely useful source of fresh water for a range of functions, such as domestic, agricultural, and industrial purposes (Asare et al. 2022). However, geogenic and anthropogenic salinisation of groundwater occurs in most aquifer systems (Biddau et al. 2019; Comte et al. 2016; Jasechko 2019; Mthembu et al. 2020; Scanlon et al. 2005; Werner et al. 2013). Groundwater salinisation refers to the process by which salt concentrations increase in groundwater, making it unsuitable for use. Groundwater salinisation can have significant economic and environmental impacts,

✉ Samuel Y. Ganyaglo
sganyaglo@yahoo.co.uk

¹ Graduate School of Nuclear and Allied Sciences, University of Ghana, Legon-Accra, Ghana

² Water Resources Research Centre, National Nuclear Research Institute, GAEC, Box LG 80, Kwabenya-Accra, Ghana

³ National Data Centre, National Nuclear Research Institute, Ghana Atomic Energy Commission, Accra, Ghana

⁴ 4Ward West Africa, P.O Box DBE 92, Daboose, Wass East, Western Region, Ghana

as it can damage crops, increase water treatment costs, and harm ecosystems (Asare et al. 2022; Hameed et al. 2019).

Several human activities often influence the quality of groundwater (Abanyie et al. 2020). Thus, it is essential to comprehend the geochemical processes that affect how dissolved ions behave in groundwater to create successful solutions to safeguard this priceless resource. Ions that are dissolved in groundwater come from a variety of natural processes, including ion exchange, interactions between rocks and water, mineral precipitation and dissolution, and evaporation (Dong and Gao 2022; Purushotham et al. 2013; Walraevens et al. 2018; Yidana et al. 2012). Moreover, human activities like mining, the use of agricultural chemicals, and sand mining may contribute more ions to the groundwater system. These human sources of pollution may significantly impact groundwater quality, necessitating the adoption of precautionary measures (Farid et al. 2013).

The use of hydrochemistry and stable isotopes to characterize the quality of groundwater and identify salination mechanisms is still an active research area (Farid et al. 2013; Spalding et al. 2019). For instance, mineralization mechanisms of groundwater in Ghana's North Densu River Basin and nitrogen pollution source identification in the upper east region of Ghana (Anornu et al. 2017; Gibrilla et al. 2010, 2022) and groundwater quality, distribution, and their health impact in Northeastern Ghana have been investigated (Asare et al. 2022).

Also, geostatistical analysis is an essential tool for groundwater studies, allowing researchers to better understand the complex relationships between groundwater resources and the environment (Carasek et al. 2020; Ene-mark et al. 2019; Hooshmand et al. 2011). A geographic information system (GIS) can be used in a variety of ways in groundwater studies. The key applications of GIS in groundwater studies include but are not limited to groundwater mapping of groundwater quality analysis to analyse the spatial distribution of water quality parameters, identify areas where groundwater may be contaminated, and develop remediation strategies.

Groundwater quality and its suitability for drinking are often assessed using an index, which gives a single value for interpretation (Abbasi and Abbasi 2012). However, the different indices each have merits and demerits, which principally arise from the weighting method. The information entropy weighting method for interpreting groundwater quality has often been utilised recently, mainly for enhancing objectiveness in weight assignment, and helps to lessen the uncertainty in weight assignment (Khatri et al. 2020).

Groundwater assessments for irrigation in many research studies are been evaluated by employing indices such as the magnesium ratio (MR), sodium adsorption ratio (SAR), Wilcox diagram, sodium percentage (Na%), and electrical conductivity (EC) (Elumalai et al. 2023; Sunkari et al. 2021).

Other proposed indices for irrigation, e.g., the irrigation water quality index (IWQI) by Meireles et al. (2010), have been applied to evaluate the suitability of water for irrigation purposes (Abbasnia et al. 2019; Abdul-Wahab et al. 2022; Iqbal et al. 2020). This index considers the physical and chemical variables to evaluate the potential problems associated with irrigated plants and soil because of phenomena such as salinization, sodification, and nutrient imbalances.

Stable isotopes of hydrogen and oxygen are extensively utilized in the field of groundwater studies to determine the origin and movement of water as well as to comprehend the mechanisms that impact groundwater quality (Gibrilla et al. 2022). Use of these isotopes is particularly advantageous because of their natural occurrence and inherent stability, ensuring that their ratios offer valuable insights into the history of water sources and the circumstances they encountered (Gibrilla et al. 2017; Adomako et al. 2015).

The complexities in gaining insight to understand the processes that influence groundwater quality and salinisation and characterise groundwater vulnerability to pollution require an integrated approach that uses hydrochemistry, stable isotopes, a multivariate statistical analysis such as principal component analysis (PCA), absolute PCA scores and multi-linear regression receptor model (APCS-MLR), geochemical modelling, and geostatistical methods to ultimately provide the needed toolbox.

The groundwater resources of the Eastern Lower Pra Basin are being severely harmed by illegal mining operations (Armah 2010), yet there is limited information about the current groundwater chemistry. Because of this information gap, it is challenging to monitor groundwater quality and develop effective management strategies for the Eastern Lower Pra Basin. Moreover, attempts to resolve the problem are further hampered by the fact that the processes behind groundwater chemistry in the semi-arid Lower Pra Basin are still little understood. It is difficult to determine the degree of pollution brought on by illicit mining operations and find practical mitigation methods without a thorough understanding of the districts' groundwater chemistry.

Additionally, the Eastern Lower Pra Basin is a significant agricultural area, with oil palm, cocoa plantation, and mining as the predominant industrial activities (Dorleku et al. 2019). Agricultural activity is the major economic activity in the district, employing about 75% of the population. Most of the crop farmers are involved in small-scale farming with an average farm size of about one acre per farmer, and large-scale farming involves the planting of crops such as cocoa, oil palm, and coffee, with oil palm being the predominant large-scale cash crop. The agricultural practices in the area may also contribute to the degradation of the groundwater quality, as the excessive use of pesticides and fertilizers can seep into the groundwater system and contaminate it.

Furthermore, the Eastern Lower Pra Basin is home to several quarry sites, including one located in Adiembra, and is still covered with outcrops that can be studied for their suitability for the quarry industry (Armah 2010; Dorleku et al. 2019). Quarry activities also have the potential to impact groundwater quality through the generation of dust and the use of chemicals during the extraction process.

The primary goals of this inquiry are to assess the chemical quality of groundwater and determine the natural and anthropogenic variables that influence groundwater quality in the semi-arid Lower Pra Basin. Use of ionic ratio graphs, multivariate statistical methods, geochemical modelling, and stable oxygen and deuterium to gain insight into quality, salination mechanism, and origin of groundwater within the Wassa district of Lower Pra Basin was employed.

2 Study area

2.1 Location, climate, and drainage features

The Wassa East District (Fig. 1a) is a region in Ghana that covers most of the Eastern Lower Pra Basin in the Western Region. It has a total population of about 102,802 and a population density of about 62.21 per km². The major industries in the area include oil palm, cocoa plantation, and mining, with small-scale mining activities in communities such as Ateiku Nsadweso, Sekyere Heman, and Sekyere Krobo. The district is characterized by an undulating landscape with an average height of about 70 m, with most parts < 150 m above sea level, and a dendritic drainage pattern with medium and small rivers and streams distributed throughout the area. The region has a warm environment, with typical yearly temperatures of 30 °C and 1500 mm of precipitation. June is the rainy month of the year, and January is the coldest. The southwest monsoon winds, which originate in the southwest and move northeastward, are primarily responsible for precipitation. March through July is the district's rainy season, while November through February is largely arid. The region is made up of gradually undulating hills with altitudes between 1000 and 1100 m above sea level, cut by a vast drainage system, and an ecotone of deteriorated wet rainforest and damp semi-deciduous forest zones. Agriculture is the major economic activity in the district, employing about 75% of the population.

2.2 Geological and hydrogeological settings

The Birimian domain of the West African Craton in Ghana includes Daboase and its surroundings, with Precambrian to Paleoproterozoic rocks present in the region (Abouchami et al. 1990). The Precambrian rocks are largely granitoids, namely Cape Coast granite, granodiorites, and

related gneisses. The Cape Coast granitoids are highly foliated, often magmatic, and potassium-rich granitoids that frequently take the form of muscovite biotite granite and granodiorites (Kesse et al. 1992). Undifferentiated biotite granitoids make up the majority of the Eastern Lower Pra Basin outcrops (Fig. 1b). The research area's southern limits are partly invaded and occupied by both biotite gneiss and undifferentiated biotite granitoids. Most of the volcanoclastics, amphiboles, migmatites, argillitic/pelitic silt, and undifferentiated biotite granitoid are interbedded. The northern portion of the research region is mostly covered by this interconnected network of rocks. At the centre parts of the region, granite and minor granodiorite seem to be intruding onto the undifferentiated biotite granitoid. Nearly the whole length of the study region is cut by an NNW-SSE trending mafic dyke or dolerite, which splits the rock groups. In places constituting the central and southwest corners of the research region, basaltic volcanic rocks, are interbedded with volcanoclastics that trend NE-SW. Typically, biotite schist and pelitic sediments encroach onto these. Nearly all of the local rocks have undergone some degree of weathering, fracture, and jointing.

The Birimian Supergroup rocks in the area, which include metavolcanic rocks, sedimentary basins, and related granitoids, dominate the hydrogeology (Fig. 1b). Because the underlying rocks are crystalline, they are naturally impervious. The consequence of this is that their hydrogeological characteristics rely on the existence and pervasiveness of secondary structures in the shapes of joints, faults, and weathered zones that provide access for recharge and storage (Banoeng-Yakubo et al. 2009).

Saprolite, saprock, and cracked bedrock are the principal locations for groundwater in the granitoid-containing Crystalline Basement Province. The zones in the Birimian with the greatest groundwater output are in the lower half of the saprolite and upper portion of the saprock, and they usually support one another concerning permeability as well as storage (Carrier et al. 2008). The higher, less permeable portion of the saprolite may act as a semi-confining layer for this productive zone, in contrast to the lower, typically saturated section of the saprolite, which is distinguished by reduced secondary clay concentration and provides a zone of improved hydraulic conductivity. Three different aquifer types may be seen in the basement rocks. These consist of fractured unweathered aquifers, fractured quartz-vein aquifers, and fractured weathered rock aquifers, all of which are linked by fractures. The subsoil, beneath the lateritic soil, the severely weathered zone, and the mildly weathered zone make up the saprolitic zone in the Crystalline Basement basins. There has been significant erosion on the saprock. The regolith is composed of both saprock and saprolite. According to statistics from a

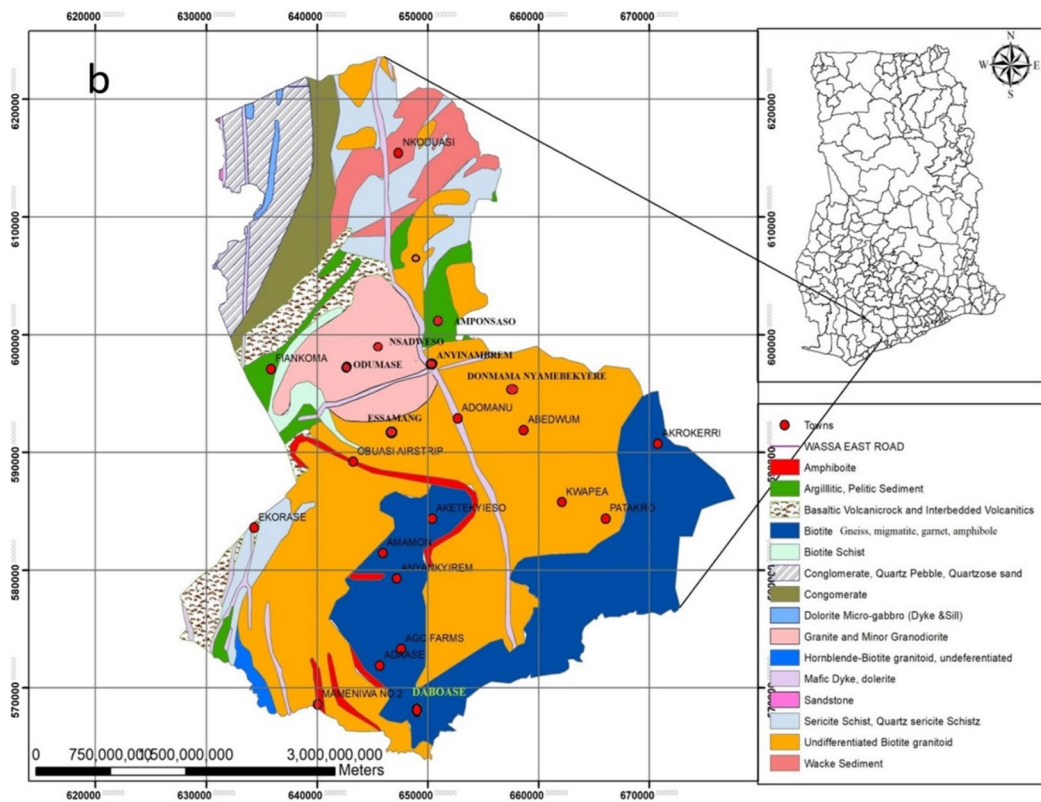
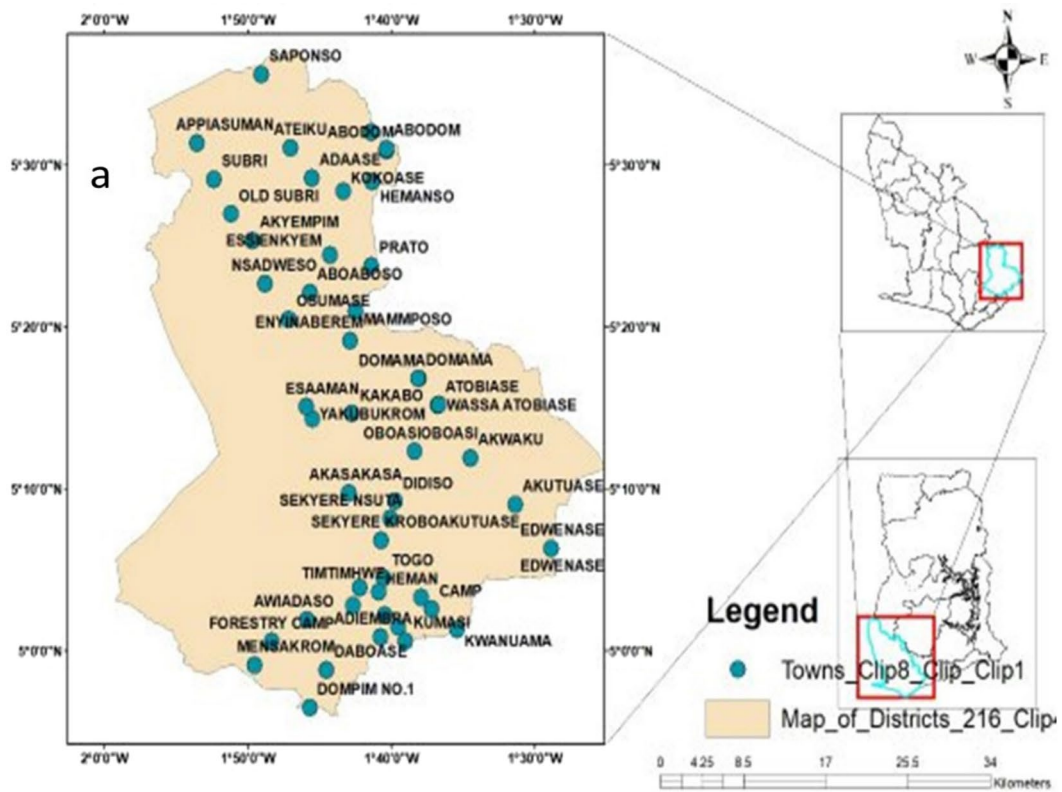


Fig. 1 Map showing **a** the study area, Wassu District, and **b** geological map

few remaining boreholes, the Lower Pra Basin outputs typically measured between 0.4 and 51.7 m³hr⁻¹, with a mean value of 4.55 m³hr⁻¹, and elevations spanned from 22 to 96 m, with a mean value of 44.2 m (ISARM-AFRICA 2004).

3 Methodology

3.1 Sampling and laboratory analysis

3.1.1 Hydrochemistry

Groundwater samples were collected in pre-cleaned 1-l high-density polyethylene (HDPE) bottles that had been acid washed with 10% nitric acid and triple rinsed with deionised water. At each sampling site, the borehole was pumped for approximately 15 min to clear stagnant water and ensure a representative sample. Bottles were rinsed three times with the sample water before filling. For cation analysis, samples were filtered on site using 0.45- μ m cellulose acetate filters and acidified to pH < 2 with ultrapure nitric acid. All samples were stored in coolers with ice packs and transported to the laboratory within 24 h of collection. Samples were then refrigerated at 4 °C until analysis, which was completed within 7 days of collection.

All analyses were performed following standard methods from the American Public Health Association (APHA 2017). The specific analytical methods and equipment used were flame photometer (Jenway PFP7, UK) for Na⁺ and K⁺ analysis. Detection limit was 0.1 mg/L for both ions. AA240FS Fast Sequential Atomic Absorption Spectrometer (Varian, USA) was used for Ca²⁺, Mg²⁺, and trace metals. Detection limits were Ca²⁺ (0.01 mg/L), Mg²⁺ (0.005 mg/L), Fe (0.01 mg/L), Pb (0.005 mg/L), Cd (0.001 mg/L), Ni (0.005 mg/L). Ion chromatograph (Dionex ICS-1100, USA) was used for anion analysis (Cl⁻, SO₄²⁻, NO₃⁻, PO₄³⁻). Detection limits were Cl⁻ (0.1 mg/L), SO₄²⁻ (0.1 mg/L), NO₃⁻ (0.05 mg/L), and PO₄³⁻ (0.02 mg/L).

Instrument calibration was performed daily using certified standard solutions. Quality control measures included analysis of method blanks, duplicate samples (10% of total samples), and certified reference materials (NIST 1643f) with each batch of samples. The relative standard deviation for duplicate analyses was < 5% for all parameters. Recovery rates for certified reference materials ranged from 95% to 100%.

For error analysis, the analytical precision, expressed as relative standard deviation (RSD) from duplicate analyses, was: major ions (< 3%), trace metals (< 5%), and nutrients (< 4%). The ionic balance error was calculated for each

sample, with all samples falling within $\pm 5\%$, indicating good data quality.

3.1.2 Stable isotopes

Groundwater samples were analysed for stable isotopes of deuterium (²H) and oxygen using 50 ml HPDE vials (¹⁸O) at 29 different sampling points. The vials were thoroughly washed with purged groundwater from the boreholes at each site, and representative samples were immediately collected and analysed by the Isotope Hydrology Laboratory at the Ghana Atomic Energy Commission to determine their stable isotope contents. To determine the molecular concentrations of ²HHO, HH¹⁸O, and HHO, the Liquid Water Isotope Analyzer (LWIA), also known as Los Gatos Research (LGR) DLT-100 (model 908-0008) equipment, was utilised to detect absorbance at a wavelength of 1390 nm. Atomic ratios of ²H/¹H and ¹⁸O/¹⁶O were derived from the molecular concentrations to determine delta-scale values relative to Vienna Standard Mean Ocean Water (VSMOW). The isotopic data were presented on a delta scale relative to VSMOW, using the equation:

$$\delta(\text{‰}) = \left(\frac{R_{\text{sample}}}{R_{\text{standard}}} - 1 \right) \times 1000 \quad (1)$$

where R_{sample} is the ratio of heavy isotope in a sample and R_{standard} the ratio of heavy isotope in standard was used to calculate the delta scale.

3.2 Water quality indices

3.2.1 Entropy-weighting groundwater quality index (IEGQI) information

The water quality index implemented in this study utilizes the entropy weighting model (Pei-Yue et al. 2010), which effectively eliminates human intervention in the assignment of indicator weights. As a result, this approach significantly enhances the objectivity of the evaluation results. Additionally, the utilization of the entropy weighting model partially resolves the uncertainty that may arise in the assignment of weight (Pei-Yue et al. 2011).

The IEGQI is given as:

$$\text{IEGQI} = \sum_{j=1}^n w_j q_j \quad (2)$$

where w_j is the entropy weight and q_j is the quality rating for each variable. Quality-rating scale (q_j) for the j th variable was estimated using the equation:

$$q_j = \frac{C_j}{S_j} \times 100 \quad (3)$$

In each water sample, C_j and S_j represent the measured concentration for each chemical variable and are compared against the respective water quality standard guidelines for drinking water set by the World Health Organization (WHO) (WHO/UNICEF 2019; WHO 2011).

The entropy weight w_j of the j th variable is given as

$$w_j = 1 - e_j / \sum_{j=1}^n (1 - e_j) \quad (4)$$

where e_j is the information entropy of the j th parameter and is given as:

$$e_j = -\frac{1}{\ln m} \sum_{i=1}^m P_{ij} \ln P_{ij} \quad (5)$$

where P_{ij} is given as

$$P_{ij} = \frac{y_{ij}}{\sum_{i=1}^m y_{ij}} \quad (6)$$

3.2.2 Irrigation water quality index (IWQI)

In this study, we assessed the suitability of groundwater quality for irrigation purposes using the Meireles et al. (2010) index, which evaluates any modifications in groundwater water quality and incorporates problems akin to irrigated plants and soil. The index is founded on two main components: (1) the application of the varimax rotation PCA to characterize the variability of irrigation water quality by variable influence and (2) the use of quality rating values (q_i) and an aggregation weight (w_i) derived after the PCA. The q_i values are then calculated by the tolerance limits as presented in Table 1 and from Eq. (7).

$$q_j = q_{j\max} - \left[\frac{(x_{ij} - x_{\text{inf}})(q_{j\text{amp}})}{x_{\text{amp}}} \right] \quad (7)$$

In Eq. (8), $q_{i\max}$ represents the maximum value of the q_i class, while x_{ij} , x_{inf} , $q_{j\text{amp}}$, and $x_{i\text{amp}}$ denote the measured

Table 2 Normalise weighting factors

Parameters	w_i
Electrical conductivity(dS/m)	0.218
HCO ₃ ⁻ (mmol/L)	0.212
Na ⁺ (mmol/L)	0.208
Cl ⁻ (mmol/L)	0.194
SAR (mmol/L) ^{1/2}	0.168
Total	1

parameter, the lower limit parameter value of the respective class, the amplitude of the q_i class, and the amplitude of the respective parameter class, respectively. The aggregation weights (w_i) of each parameter were derived from the PCA/factor analysis (PCA/FA), and these w_i values were normalized to one, as shown in Table 2.

$$w_j = \sum_{p=1}^k F_p A_{jp} / \sum_{p=1}^k \sum_{j=1}^n F_p A_{jp} \quad (8)$$

The parameter weight (w_i) is given by the product of the component (F) and the variable j by factor p explicability (A_{jp}), where j represents the number of selected model parameters ranging from 1 to n , and p represents the number of selected model factors ranging from 1 to k . The IWQI was calculated as follows:

$$\text{IWQI} = \sum_{i=1}^n q_i w_j \quad (9)$$

where q_j is the j th parameter quality value, and w_j is the standardised j th variable weight. The IWQI values are scaled between 0 and 100 and classified as presented in Table 3.

3.3 Multivariate statistical techniques

3.3.1 Principal component analysis (PCA)

To improve comprehension and analysis of datasets, PCA is a mathematical approach that may successfully decrease the dimensionality of variables. It uses orthogonal transformations as a multivariate statistical analysis technique to create principal components from a collection of observations of

Table 1 Tolerance limit for quality measurement (q_i) calculation

q_i	Electrical conductivity(dS/m)	SAR (mmol/L) ^{1/2}	Na ⁺ (mmol/L)	Cl ⁻ (mmol/L)	HCO ₃ ⁻ (mmol/L)
85–100	0.20 ≤ EC < 0.75	2 ≤ SAR < 3	2 ≤ Na ⁺ < 3	1 ≤ Cl ⁻ < 4	1 ≤ HCO ₃ ⁻ < 1.5
60–85	0.75 ≤ EC < 1.50	3 ≤ SAR < 6	3 ≤ Na ⁺ < 6	4 ≤ Cl ⁻ < 7	1.5 ≤ HCO ₃ ⁻ < 4.5
35–60	1.50 ≤ EC < 3.00	6 ≤ SAR < 12	6 ≤ Na ⁺ < 12	7 ≤ Cl ⁻ < 10	4.5 ≤ HCO ₃ ⁻ < 8.5
0–35	EC < 0.20 or EC ≥ 3.00	SAR < 2 or SAR ≥ 12	Na ⁺ < 2 or Na ⁺ ≥ 9	Cl ⁻ < 1 or Cl ⁻ ≥ 10	HCO ₃ ⁻ < 1 or HCO ₃ ⁻ ≥ 8.5

Table 3 IWQI Classifications and characteristics (Meireles et al. 2010)

IWQI values	Explanation	Recommendation	
		Soil	Plant
85–100	No restriction (NR)	Excellent for almost all types of soil. Soil is exposed to lower risks of salinity/sodicity problems	No toxicity risk for most plants elevated
70–85	Low restriction (LR)	Suitable for irrigated soils with a light texture or moderate permeability, and require soil leaching is recommended to avoid soil sodicity in heavy textures	Elevated risks for salt-sensitive plants
55–70	Moderate restriction (MR)	Better suited for soils with moderate to high permeability values, and to avoid soil degradation, moderate leaching of salts is highly recommended	Plants with moderate tolerance to salts maybe grow
40–55	High restriction (HR)	Suited for soils with high permeability without compact layers, with high-frequency irrigation schedule	Suitable for irrigation of plants with moderate to high tolerance to salts with special salinity control practices, except water with low Na ⁺ , Cl ⁻ , and HCO ₃ ⁻ values
0–40	Severe restriction (SR)	Not suitable for irrigation in soil under normal conditions	Only plants with high salt tolerance, except for waters with extremely low values of Na ⁺ , Cl ⁻ , and HCO ₃ ⁻

potentially associated variables (PCs). These essential elements may be stated as follows:

$$Z_{ik} = \partial_{i1}X_{1k} + \partial_{i2}X_{2k} + \dots + \partial_{im}X_{mk} \tag{10}$$

X stands for the variables measured, Z for its component score, *i* for its component number, *k* for its sample size, and *m* for the overall number of variables. The data were subjected to the Kaiser-Meyer-Olkin (KMO) tests and the KMO value of 0.56 was obtained, which was permissible (> 0.5) for PCA analysis (Kaiser 1991). The number of components was determined solely by Kaiser’s formula, which eliminates any components with eigenvalues < 1.0.

3.3.2 The APCS-MLR receptor model

The APCS-MLR receptor model has been widely employed in pollution source apportionment studies, particularly in the analysis of groundwater, over the years (Su et al. 2021). The model’s effectiveness in identifying the sources of pollution has contributed to its frequent use in these studies (Gholizadeh et al. 2016; Meng et al. 2018; Yu et al. 2022). The approach of determining the absolute principal component score (APCS) involves utilizing the output of the PCA and performing a multivariate linear regression (MLR) that utilizes the APCS values as independent variables and measured pollutant concentrations as dependent variables. The regression coefficient values determine the relative contributions of different sources of pollution. The APCS-MLR model is formulated using Eqs. (11–18).

$$C_{ik} = b_{i0} + \sum_{p=1}^P b_{ip} \times APCS_{pk} \tag{11}$$

where *i* denotes the water quality variables count analysed, *k* denotes the observation count, and *p* denotes the factors of the water quality variables, *C_{ik}* denotes the *i*th parameter for sample *k* concentration, and *b_{i0}* denotes MLR constant, *b_{ip}* denotes the source *p* regression coefficient, and *APCS_{pk}* is the absolute component. *APCS_{pk}* is obtained by Eqs. (12–16)

$$(Z_i)_j = C_{ij} - \frac{C_j}{\sigma_j} \tag{12}$$

$$(Z_o)_j = (0 - C_j) / \sigma_j \tag{13}$$

$$(A_o)_j = \sum_{p=1}^P S_{jp} Z_{oj} \tag{14}$$

$$(A_z)_{ip} = \sum_{p=1}^P S_{jp} Z_{ij} \tag{15}$$

$$APCS_{ip} = (A_z)_{ip} - A_{0j} \tag{16}$$

where *(Z_k)_i* is the normalised *j*th variable of the *i*th sample, *(Z_o)_j* is the absolute zero concentration normalised value of the *j*th variable, \bar{C}_j and σ_j are respectively the mean and standard deviation of the *i*th variable, *S_{jp}* is the *p*th component for the *j*th variable score coefficient, *(A_z)_{ip}* is the component score for the *i*th sample of the *p* component, *(A₀)_j* is

the component absolute zero concentration, and $APCS_{ip}$ is the absolute component score in the APCS-MLR model.

The percentage source contribution (PC_p) was calculated using an absolute value method (Gholizadeh et al. 2016), which typically results in negative values of $b_{ij} \times APCS_{pk}$ indicating a source's negative contribution of over 100%. The formula for calculating PC_p is given as:

$$PC_p = \frac{|b_{ip} \times \overline{APCS}_{pk}|}{b_{i0} + \sum_p |b_{ip} \times \overline{APCS}_{pk}|} \quad (17)$$

The percentage of contribution from an unidentified source, PC_j is expressed by the formula

$$PC_j = \frac{|b_{ip}|}{b_{i0} + \sum_p |b_{ip} \times \overline{APCS}_{pk}|} \quad (18)$$

where \overline{APCS}_{pk} is the average of the absolute principal component.

3.4 Saturation indices

PHREEQC was used to calculate saturation indices (SI) for different mineral phases in groundwater. The calculation relied on an equation that considered the ion activity product (IAP) and solubility product (K_{sp}) at a specific temperature.

Given by the equation:

$$SI = \log\left(\frac{IAP}{K_{sp}}\right) \quad (19)$$

A negative SI value suggested that the groundwater had lower concentrations of a specific mineral, indicating it was under-saturated and had shorter residence times (Mohanty et al. 2018). A positive SI value, on the other hand, meant that the groundwater was supersaturated concerning the mineral in solution and could not further dissolve that mineral.

3.5 Geostatistics

In this study, geostatistical analysis was performed using Empirical Bayesian Kriging (EBK) in the ArcGIS program (version 10.7). This method's advantage is that it uses iterative simulations based on Bayes' rule to continuously assess the inaccuracy generated in semi-variogram model estimation (Gribov and Krivoruchko 2020; Omre 1987). Compared to previous kriging approaches, this method requires less interactive modelling, provides accurate standard prediction errors, allows for more accurate forecasts of slightly nonstationary data, and delivers better forecasts for small

datasets (Samsonova et al. 2017). The model power semi-variogram was selected, and a total of 100 simulations of the geostatistical analysis were performed. This choice was made because of its relatively rapid execution, flexibility, and average performance and correctness.

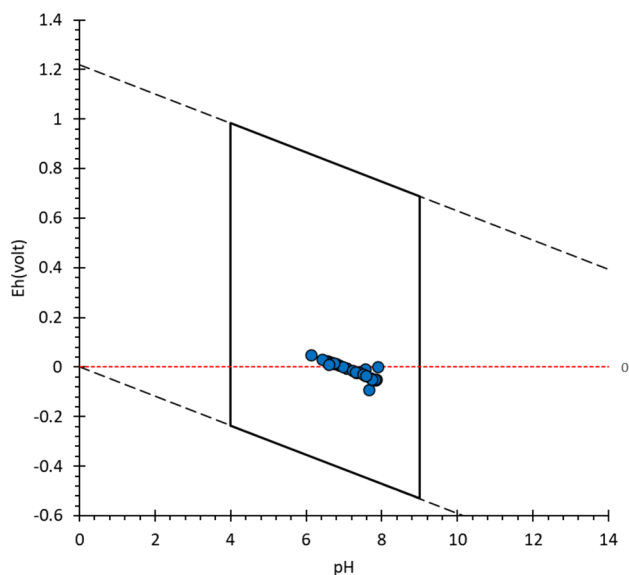
4 Results

4.1 Physicochemical characterization

The measured physio-chemical variables of groundwater sampled from the study area were compared with World Health Organization guidelines and are summarised in Table 4. The samples were in general warm with an average temperature of 28.62 °C and ranged from 26.30 to 30.90 °C. Groundwater samples' Eh values ranged between -0.092 and 0.0493 V with an average of -0.0104 V. Sixteen of the samples (55.7%) had negative redox (Eh) values, implying a reducing environment for the sampled groundwater, whereas 13 (13) samples forming 41.38% of the remaining samples showed positive Eh values indication oxidising environment for the sampled groundwater (Fig. 2). Groundwater pH values ranged from 6.13 to 7.89; however, about 6.9% of the groundwater samples (BH7 and BH12) were outside the WHO recommended limits (6.5–8.5). Groundwater samples' electrical conductivity (EC) values were generally all within the WHO acceptable limit (2500 μ S/cm); the samples' EC values varied from 79.6 to 1086 μ S/cm with a mean value of 278.5 μ S/cm. On average, the groundwater TDS was 160.48 mg/L and can be classified as freshwater (< 1000 mg/l). The total dissolved solids (TDS) ranged between 40 mg/l obtained from BH7 (Sekyere Aboaboaso) to 549 mg/l obtained from BH11 (Anyinabrim) and when compared to guideline values were all within WHO acceptable limits. The high TDS values of groundwater in Anyinabrim recorded indicate longer water-rock interaction coupled with anthropogenic influences as there was a very strong positive correlation ($R > 0.75$, $p < 0.05$) between TDS and Cl^- , SO_4^{2-} and PO_4^{3-} . The major cation Ca^{2+} , Mg^{2+} , Na^+ , and K^+ averages were 15.60, 3.22, 22.62, and 9.51 mg/L, with ranges of 3.37–48.03, 0.28–22.56, 43.30–122.90, and 3.10–25.10 mg/L, respectively, with all within the WHO acceptable limits. On average, the trend of ion dominance was $Na^+ > Ca^{2+} > K^+ > Mg^{2+}$ for the cations and agreed with similar studies by Armah et al. (2010) within the study area. The strong and positive correlation between Na^+ and TDS may give a clue that the geochemical source of the ion may be due to the rock-water interaction. Also, the strong and positive correlation between Na^+ and ions such as Cl^- , PO_4^{3-} , and SO_4^{2-} ($R > 0.75$, $p < 0.05$) may indicate that Na^+ ions may be not only sourced from geogenic origin but also from anthropogenic influences. The mean

Table 4 Statistical summary of physicochemical parameters measured in the sample groundwater

Variable	Minimum	Maximum	Mean	Std. deviation	WHO limits	Percentage outside the WHO limit
Temp (°C)	20.50	30.90	28.42	1.822	–	–
pH	6.130	7.890	7.167	0.503	6.5–8.5	6.9
Eh (V)	–0.092	0.049	–0.010	0.031	–	–
EC (μS/cm)	79.60	1086	278.5	204.2	25,000	0
TDS (mg/L)	40.00	597.0	160.5	114.5	1000	0
HCO ₃ [–] (mg/L)	16.00	290.0	80.24	59.32	120	20.7
Na ⁺ (mg/L)	4.300	122.9	22.62	23.10	200	0
K ⁺ (mg/L)	3.100	25.10	9.514	5.981	164	0
Ca ²⁺ (mg/L)	3.367	48.03	15.60	10.10	75	0
Mg ²⁺ (mg/L)	0.280	22.56	3.219	4.516	30	0
Cl [–] (mg/L)	6.993	85.97	24.82	17.16	250	0
NO ₃ [–] (mg/L)	0.031	2.999	0.758	0.888	50	0
PO ₄ ^{3–} (mg/L)	0.002	0.670	0.046	0.123	10	0
SO ₄ ^{2–} (mg/L)	0.139	19.72	1.739	3.548	250	0
Fe (mg/L)	0.104	2.015	0.315	0.341	0.3	44.8
Pb (mg/L)	bdl	0.196	0.038	0.056	0.01	44.8
Cd (mg/L)	bdl	0.216	0.023	0.054	0.003	17.2
Ni (mg/L)	bdl	0.340	0.043	0.079	0.02	51.7
δ ² H (‰, VSMOW)	–10.35	–2.00	–6.75	–	–	–
δ ¹⁸ O (‰, VSMOW)	–2.82	–1.58	–2.24	–	–	–

**Fig. 2** Plot of Eh versus pH

concentrations of the dissolved anions in the groundwater system, HCO₃[–], Cl[–], SO₄^{2–}, PO₄^{3–}, and NO₃[–], were 80.24, 24.82, 1.74, 0.05, and 0.76 mg/L, respectively. The minimum and maximum concentrations of the anions HCO₃[–], Cl[–], SO₄^{2–}, PO₄^{3–}, and NO₃[–] ranged from 16.00 to 290.0,

6.99–85.97, 0.14–19.72, 0.001–0.67, and 0.03–2.95 mg/L, respectively, with only 20.7% of groundwater sampled measured for HCO₃[–], above the WHO acceptable limit of 120 mg/L. The trend of anion dominance was in the order HCO₃[–] > Cl[–] > SO₄^{2–} > NO₃[–] > PO₄^{3–}; also a similar trend of relative abundances of major anions was observed by Armah et al. (2010) within the district (Table 5).

In the sampled groundwater, bicarbonate (HCO₃[–]) may be controlled according to Loh et al. (2020), the reaction between CO₂ gas in the soil and atmosphere forming carbonic acid in the soil water, which chemically dissolves feldspars and plagioclase in different types of rock during infiltration. The sampled groundwater NO₃[–] concentrations were averagely low (< 5 mg/L) although there were farming activities in the study area. However, there is a weak and positive correlation between NO₃[–] and Eh, and this may indicate that NO₃[–] concentration may be influenced by redox conditions. For heavy metals, a total of nine trace elements Zn, Fe, Cu, Cr, Cd, Ni, Co, Pb, and As, were analysed to determine the quality of groundwater in the study area. However, As, Cr, Zn, Co, and Cu were below the detection limit. On average, Fe, Pb, Cd, and Ni were 0.315, 0.38, 0.0227, and 0.0431 mg/L, each ranging from 0.104 to 2.015 mg/l, bdl to 0.196, bdl to 0.216 mg/L, and bdl to 0.34 mg/L respectively. On average, the trend of the heavy metals concentrations

Table 5 Comparison of the parameter's concentrations in sampled groundwater with other studies within the study area

Country	HCO ₃ ⁻	Cl ⁻	SO ₄ ²⁻	NO ₃ ⁻	PO ₄ ³⁻	Na ⁺	K ⁺	Mg ²⁺	Ca ²⁺	References
Lower Pra	43.90–300.8	10.60–715.1	18.10–266.9	0.09–9.03	0.02–0.19	22.6–697.5	3.10–52.0	2.86–25.38	5.98–29.50	Armah et al. (2010)
Lower Pra	–	–	1.6–96.2	0.08–5.01	0.01–3.08	–	–	–	–	Dorleku et al. (2019)
Lower Pra	16–290	6.99–85.97	0.139–19.92	0.031–2.999	0.002–0.670	4.3–122.9	3.1–25.10	0.280–22.56	3.37–48.03	Present study

was Pb > Fe > Ni > Cd. About 44.8%, 44.8%, 51.7%, and 17.2% of the sampled groundwater, respectively, had elevated concentrations of Pb, Fe, Ni, and Cd above the WHO acceptable limit. Cd correlated moderately positively and poorly positively with Ca²⁺ ($R=0.60$, $p<0.05$) and Mg²⁺ ($R=0.39$, $p<0.05$), respectively (Table 6), implying factors that control Ca²⁺ and Mg²⁺ concentration may also control Cd concentration.

4.2 Stable isotopes of ²H and ¹⁸O

The summary statistics of the isotopic composition of the groundwater sampled are presented in the Table 4. Considering the table, the stable isotope composition of the sampled groundwater ranged between –2.82 and –1.58‰ VSMOW for δ¹⁸O, with a mean of –2.24‰ VSMOW. The delta deuterium (δ²H) values ranged from –10.35 to –2‰ VSMOW, with a mean of –6.75‰ VSMOW.

4.3 Hydrochemical facies

The hydrochemical facies define the distinguishing chemical characteristics of water solutions in hydrological systems (Ram et al. 2021). The facies depict the results of interactions between groundwater and the rocks that make up the lithological structure. Various processes, including weathering, ion exchange, mixing, and evaporation, can lead to the evolution of hydrochemical facies in a granitic aquifer. An alternative to the traditional Piper diagram was introduced by Shelton et al. (2018), utilizing isometric log ratios (ilr) of major ions, to classify water types on an ilr-ion plot. This approach, based on compositional data analysis, may provide a more precise and reliable means of water type classification in hydrogeochemical studies. The method involves the computation of four ilr values (z_1 , z_2 , z_3 , and z_4) using the equation:

$$z_1 = \sqrt{\frac{2}{3}} \ln \frac{\sqrt{[\text{Ca}^{2+}][\text{Mg}^{2+}]}}{[\text{Na}^+ + \text{K}^+]}$$
 (20)

$$z_2 = \frac{1}{\sqrt{2}} \ln \frac{[\text{Ca}^{2+}]}{[\text{Mg}^{2+}]}$$
 (21)

$$z_3 = \sqrt{\frac{2}{3}} \ln \frac{\sqrt{[\text{Cl}^-][\text{SO}_4^{2-}]}}{[\text{HCO}_3^- + \text{CO}_3^{2-}]}$$
 (22)

and

$$z_4 = \frac{1}{\sqrt{2}} \ln \frac{[\text{Cl}^-]}{[\text{SO}_4^{2-}]}$$
 (23)

Table 6 Pearson correlation matrix of the physicochemical variables

Variables	Temp(°C)	pH	Eh	EC	TDS	HCO ₃ ⁻	Na ⁺	K ⁺	Ca ²⁺	Mg ²⁺	Cl ⁻	NO ₃ ⁻	PO ₄ ³⁻	SO ₄ ²⁻	Fe	Pb	Cd	Ni
Temp(°C)	1	0.429	-0.396	0.242	0.258	0.292	0.181	0.319	0.279	0.136	0.170	-0.220	-0.120	0.044	-0.046	0.117	0.220	0.196
pH	0.429	1	-0.877	0.360	0.417	0.476	0.216	0.343	0.519	0.367	0.288	-0.414	0.044	0.072	0.160	0.102	0.314	0.171
Eh	-0.396	-0.877	1	-0.212	-0.243	-0.286	-0.193	-0.290	-0.193	-0.094	-0.094	0.400	-0.065	-0.065	-0.156	-0.044	-0.106	-0.221
EC	0.242	0.360	-0.212	1	0.970	0.950	0.883	0.777	0.753	0.619	0.898	-0.021	0.747	0.842	-0.079	0.149	0.079	-0.014
TDS	0.258	0.417	-0.243	0.970	1	0.989	0.902	0.780	0.782	0.614	0.895	-0.070	0.711	0.807	0.084	0.117	0.153	-0.025
HCO ₃ ⁻	0.292	0.476	-0.286	0.950	0.989	1	0.874	0.787	0.782	0.608	0.836	-0.113	0.656	0.750	0.112	0.126	0.159	0.013
Na ⁺	0.181	0.216	-0.193	0.883	0.902	0.874	1	0.764	0.471	0.313	0.763	0.029	0.810	0.883	0.044	0.139	-0.093	-0.057
K ⁺	0.319	0.343	-0.290	0.777	0.780	0.787	0.764	1	0.499	0.197	0.583	-0.146	0.492	0.611	-0.046	-0.005	-0.097	0.224
Ca ²⁺	0.279	0.519	-0.193	0.753	0.782	0.782	0.471	0.499	1	0.721	0.813	-0.115	0.308	0.408	0.009	0.012	0.388	-0.061
Mg ²⁺	0.136	0.367	-0.094	0.619	0.614	0.608	0.313	0.197	0.721	1	0.709	-0.172	0.383	0.438	0.079	0.145	0.596	-0.043
Cl ⁻	0.170	0.288	-0.094	0.898	0.895	0.836	0.763	0.583	0.813	0.709	1	-0.007	0.674	0.757	-0.090	0.086	0.313	-0.117
NO ₃ ⁻	-0.220	-0.414	0.400	-0.021	-0.070	-0.113	0.029	-0.146	-0.115	-0.172	-0.007	1	0.025	0.008	-0.169	-0.245	-0.258	-0.106
PO ₄ ³⁻	-0.120	0.044	-0.065	0.747	0.711	0.656	0.810	0.492	0.308	0.383	0.674	0.025	1	0.953	-0.047	0.274	-0.123	-0.074
SO ₄ ²⁻	0.044	0.072	-0.065	0.842	0.807	0.750	0.883	0.611	0.408	0.438	0.757	0.008	0.953	1	-0.004	0.225	-0.090	-0.118
Fe	-0.046	0.160	-0.156	-0.079	0.084	0.112	0.044	-0.046	0.009	0.079	-0.090	-0.169	-0.047	-0.004	1	-0.062	0.043	-0.148
Pb	0.117	0.102	-0.044	0.149	0.117	0.126	0.139	-0.005	0.012	0.145	0.086	-0.245	0.274	0.225	-0.062	1	0.014	-0.100
Cd	0.220	0.314	-0.106	0.079	0.153	0.159	-0.093	-0.097	0.388	0.596	0.313	-0.258	-0.123	-0.090	0.043	0.014	1	-0.062
Ni	0.196	0.171	-0.221	-0.014	-0.025	0.013	-0.057	0.224	-0.061	-0.043	-0.117	-0.106	-0.074	-0.118	-0.148	-0.100	-0.062	1

Bold highlights r values greater than ±0.5 and are significantly correlated

Fig. 3 Isometric log ratio (ilr) to display the observed water type of the sampled groundwater

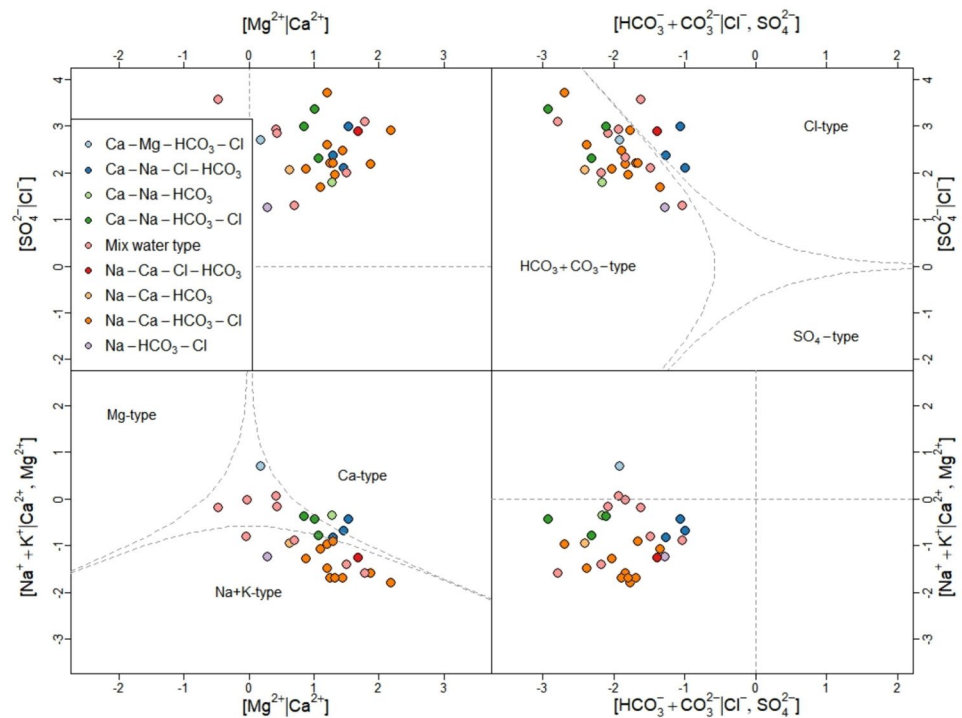


Table 7 Sampled groundwater quality classifications for drinking

Classification	Count per classification	Percentage (%)
Average	4	14.3
Excellent	15	53.6
Extremely poor	3	10.7
Good	4	14.3
Poor	2	7.1

where all concentrations are expressed as meq/L.

The hydrochemical facies of the sampled groundwater observed (Fig. 3) were Ca–Mg–HCO₃–Cl (3.5%) resulting from fresh groundwater with minimal rock–water interaction, Ca–Na–HCO₃ (3.5%) and Na–Ca–HCO₃ (3.5%) as a consequence of significant ion exchange processes, Ca–Na–HCO₃–Cl (10.2%) and Na–Ca–HCO₃–Cl (34.5%) depicting groundwater influenced more by silicate rock weathering, anthropogenic impacts, and mixing of different groundwater sources with higher chloride concentrations, mix water type (27.6%) groundwater with no ion dominance, and Na–HCO₃–Cl (3.5%), Ca–Na–Cl–HCO₃ (10.2%), and Na–Ca–Cl–HCO₃ (3.5%) groundwater with further ion exchange processes.

4.4 Groundwater quality

Assessing the quality of groundwater for drinking purposes is critical, as it has a significant impact on human health. To achieve this, the information entropy water quality index was employed to provide values that help in interpreting the groundwater quality. From Table 7, about 53.6% of the groundwater samples were classified as excellent quality. About 14.3% of the sampled groundwater was classified as good quality and 14.3% as average quality, indicating that they are still safe for drinking. Nonetheless, it was found that 7.1% of the samples were of poor quality, and about 10.7% of the samples, specifically from boreholes BH1, BH2, BH3, and BH4, were categorised as being of extremely poor quality. These boreholes are all located within the mining community of Domama. Spatially, excellent water quality was predicted around the western north (which is characterised by high elevation) and the western south portion of the study area. However, the IEQWI values predicted using empirical Bayesian kriging suggest that the eastern part of the study area, particularly in communities such as Amponsaso, Oseikrom, Atwerebasa, and Abetemansu, had extremely poor groundwater quality (Fig. 4a). These spatial variations in water quality can be attributed to the differences in human activities across the region. Aside from mining activity by large corporations, small-scale (artisanal) gold mining has been identified as a major human activity influencing the groundwater quality in the basin (Dorleku et al. 2018).

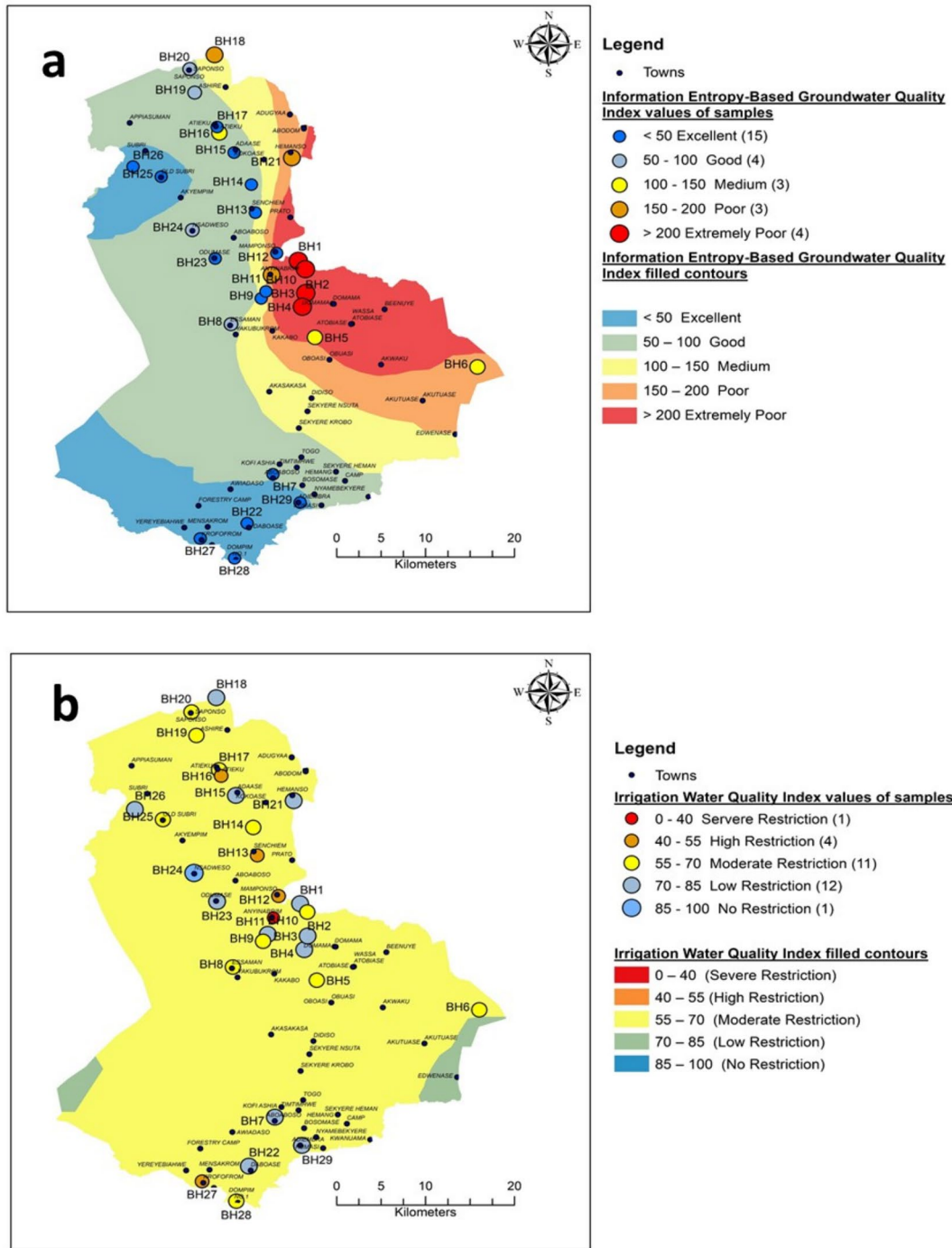


Fig. 4 EBK kriging prediction map for a IEBGWI values and b IWQI

Table 8 presents the assessment of the quality of groundwater for irrigation purposes, which is another vital factor to consider, using the IWQI. According to the results, only a minor proportion of the groundwater

samples, approximately 3.45%, fell under the no-restriction zone, indicating that they can be used safely for irrigation purposes without any treatment. However, 13.8% of the samples were in the high restriction zone, while

Table 8 Sampled groundwater quality classifications for irrigation

Categories	Frequency	Percentage (%)
High restriction	4	13.8
Low restriction	12	41.4
Moderate restriction	11	37.9
No restriction	1	3.45
Severe restriction	1	3.45

37.9% were in the moderate restriction zone. A concerning 3.45% of the samples were in the severe restriction zone, indicating that they are not suitable for irrigation at all. Nonetheless, the larger part of the samples, about 41.4%, were classified as low restriction, meaning that they are relatively safe to use for irrigation but some treatment may be necessary. Spatially, the EBK predicted a large part of the district was classified as irrigation water with moderate restriction (Fig. 4b).

4.5 Groundwater salinization source identification from PCA

PCA was used as a complementary tool to provide a prior insight into hidden factors in the hydrochemical dataset; the PCA result is presented in Table 9. The first component explains about 42.3% variation of the hydrochemical data and showed a strong positive correlation with EC, HCO₃⁻,

Na, K, Cl, and SO₄, moderate positive correlation with Mg, and weak positive correlation with pH. Component 2 explains about 14.8% variance of the hydrochemistry and shows a moderate and positive correlation with Cd and pH, weak but positive correlation with temperature, Ca, and Mg, moderate and negative association with NO₃⁻, and lastly weak and negative correlation with PO₄³⁻ and SO₄²⁻. Component 3 explains about 9.8% of the data and correlated moderately positively with Ni, weakly positively with temperature, and K, and weakly negatively with Mg and Cd. Component 4, which explains 8% of the data, correlated moderately positively with Fe, weakly positively with Pb, and moderately negatively with nitrate. Lastly, component 5 explains about 7% and correlated strongly positively with Fe and moderately negatively with Pb.

The variation in groundwater chemistry appears to be influenced by multiple factors, as suggested by the PCA outcome. The first component seems to be associated with salinity and shows a strong correlation with electrical conductivity (EC) and major ions, including HCO₃⁻, Na⁺, K⁺, Cl⁻, and SO₄²⁻. These observations may indicate that the groundwater is impacted by the geogenic mechanism of mineralization through mineral dissolution and/or interactions between water and rocks, leading to the release of these ions into the groundwater (Argamasilla et al. 2017; Jasrotia et al. 2019).

The second component appears to be related to the presence of trace metals as well as the pH of the groundwater.

Table 9 Varimax rotation principal component variable correlation and eigen values

Parameter	Principal component				
	1	2	3	4	5
Temp	0.278	0.489	0.47	-0.02	-0.141
pH	0.436	0.64	0.26	0.11	0.142
EC	0.979	-0.105	0.04	-0.08	-0.031
HCO ₃ ⁻	0.964	0.04	0.07	-0.03	0.139
Na ⁺	0.878	-0.343	0.14	0.06	0.117
K ⁺	0.756	-0.101	0.49	-0.09	0.128
Ca ²⁺	0.777	0.368	-0.17	-0.26	0.032
Mg ²⁺	0.667	0.402	-0.45	-0.08	-0.114
Cl ⁻	0.919	0.003	-0.23	-0.18	-0.083
NO ₃ ⁻	-0.128	-0.536	-0.19	-0.57	-0.009
PO ₄ ³⁻	0.758	-0.492	-0.09	0.22	-0.085
SO ₄ ²⁻	0.846	-0.429	-0.05	0.16	-0.022
Fe	0.009	0.174	-0.15	0.37	0.83
Pb	0.187	0.006	-0.05	0.73	-0.512
Cd	0.195	0.709	-0.44	-0.13	-0.16
Ni	-0.019	0.174	0.68	-0.22	-0.155
Eigen value	6.8	2.4	1.6	1.3	1.1
Percentage variance	42.3	14.8	9.8	8.0	7.0
Percentage cumulative variance	42.3	57.1	66.9	74.9	81.9

* Values in bold indicate the most influential variables to each PCs

The positive correlation between cadmium (Cd) and pH suggests that there may be anthropogenic sources such as mining activities (Armah 2010). The mining industry is a significant source of cadmium pollution. The negative correlation with nitrate (NO_3^-) and phosphate (PO_4^{3-}) may suggest that these ions are being removed from the groundwater.

The third component appears to be related to the presence of Ni and K^+ as well as temperature. The positive correlation with Ni and K^+ may suggest that these elements are derived from geogenic sources, such as the mineral weathering of pyroxenes (Armah 2010). The positive correlation with temperature may indicate that there is a temperature-dependent process. One possible factor that could explain the association between Ni and K^+ in groundwater from a granitic aquifer is the presence of mica and pyroxene minerals in the underlying rock. Mica is a common mineral in granitic rocks and can contain significant amounts of both potassium and nickel. As mica minerals weather and break down, they can release both K^+ and Ni into groundwater, leading to their co-occurrence in the aquifer (Bari et al. 2021). In general, the relationship among Ni, K^+ , and temperature in groundwater is likely to be influenced by a combination of factors and will require further research to determine the specific factors involved in this relationship. This component can be described as a Ni contamination source. The fourth

component appears to be related to iron (Fe), lead (Pb), and nitrate (NO_3^-). The positive correlation of the component with Fe and Pb may suggest that these elements are derived from anthropogenic sources, such as quarry activities (Snousy et al. 2020). The negative correlation with nitrate (NO_3^-) may suggest that the fourth component is unrelated to anthropogenic factors such as farming activities that may be influencing the groundwater. The fifth component appears to be related to iron (Fe) and lead (Pb), with a strong positive correlation with Fe and a moderate negative correlation with Pb. This suggests processes that to a lesser degree influence dissolution of iron-rich minerals in the aquifer (Halim et al. 2010). Overall, the PCA result suggests that a combination of natural and anthropogenic sources, including mining and quarrying activities, affects the water quality.

4.6 Spatial distribution of PCA factors

Figure 5 presents the spatial distribution of the factor scores of the sampled groundwaters based on the EBK. Component 1, which is characterized by natural mechanisms of groundwater salinization, was evenly distributed with average values throughout the district. However, higher values were observed in the communities of Anyinabrim and Amponsaso located around the eastern fringes

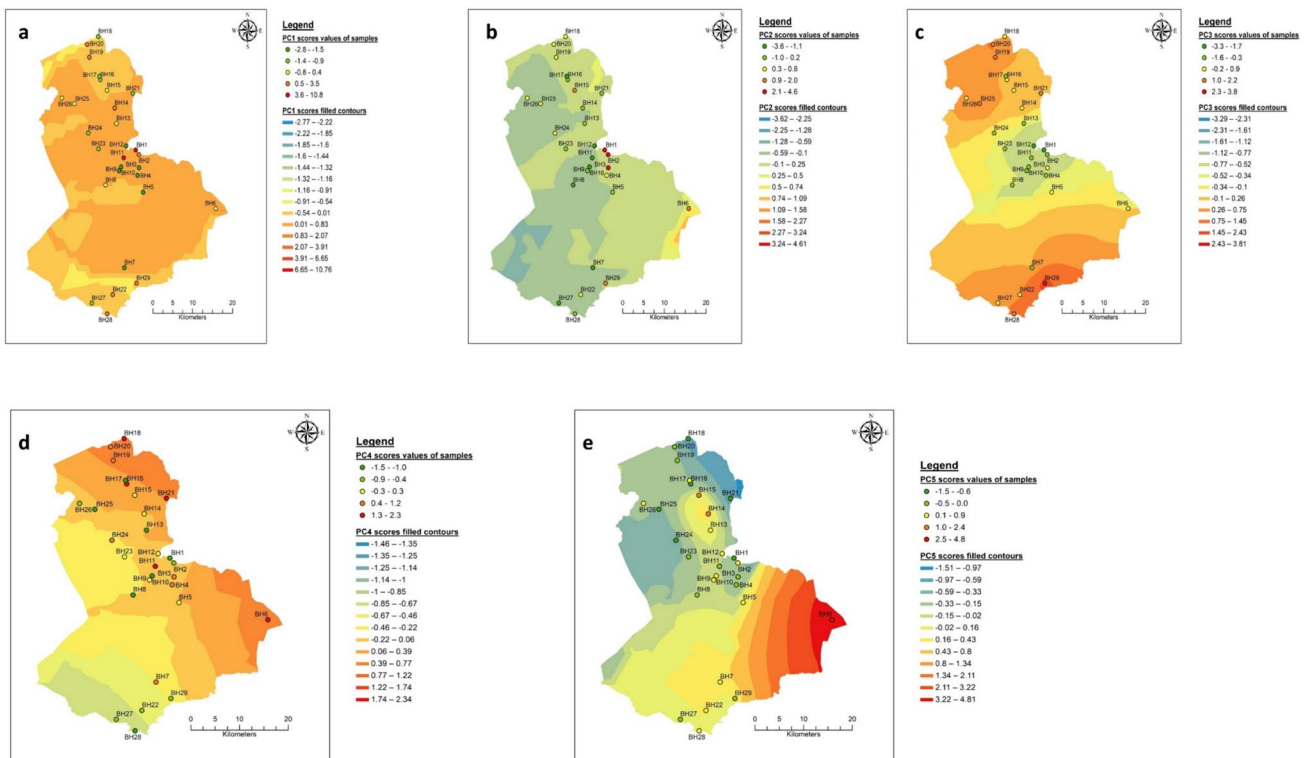


Fig. 5 EBK prediction mapping of the five principal component scores; **a** PC1; **b** PC2; **c** PC3; **d** PC4; **e** PC5

(Fig. 5a). Component 2, which is depicted by Cd contamination, was most prevalent in the eastern and southeastern portions of the district with high scores, particularly in communities with BH1, BH2, BH3, and BH6 (Fig. 5b).

Also, high scores of the third component were mainly found in the northern and southern regions of the district, particularly in boreholes BH19, BH20, and BH26 in the north and BH28 and BH29 in the south. This component illustrates nickel (Ni) contamination (Fig. 5c). The fourth component, related to high iron (Fe) and lead (Pb) derived from anthropogenic sources, was evenly distributed with high values around the northeastern and southeastern parts of the district, with more pronounced values in boreholes BH18, BH21, and BH6 (Fig. 5d). Lastly, component 5, which represents processes that may influence the dissolution of iron-rich minerals in the aquifer to a lesser degree, was more pronounced around the southeastern peripheries, particularly in borehole BH6 (Fig. 5e).

4.7 Salinization source apportionment-based APCS-MLR

The chemistry of groundwater is typically influenced by a range of factors (Walraevens et al. 2018). Table 10 and Fig. 6 present the contributions of sources of the five factors identified by the PCA using the APCS-MLR receptor model. The APCS-MLR receptor model suggests a well-fitted relationship between the observed and predicted values, with R^2 generally > 0.5. The R^2 for the model was 0.8, indicating a

good level of accuracy in predicting the values. About 19.4% of groundwater pollution is contributed on average by factor 1 (Fig. 6a), representing mineral dissolution and weathering, resulting from high contribution rates of EC (67%), K^+ (30.3%), Ca^{2+} (42.3%), Mg^{2+} (37.8%), PO_4^{3-} (34%), and SO_4^{2-} (46%), as shown in the table (Fig. 6b). Factor 2, represented by trace metal contamination, primarily Cd, contributed on average 16% to the total pollution sources, resulting from Na^+ (40.8%), Ca^{2+} (28.9%), NO_3^- (20.83%), PO_4^{3-} (35.6%), SO_4^{2-} (33.6%), and the highest percentage of Cd (45.6%). The third factor shows nickel contamination contributed on average 14.6% to total groundwater pollution, resulting from high contribution rates of Na^+ (19.3%), K^+ (33%), Mg^{2+} (20.6%), Cl^- (30.9%), Cd (33.4%), and Ni (44.8%). The contribution of Factor 4, which represents anthropogenic sources such as quarrying and urbanisation, accounted for approximately 12.8% of the total groundwater pollution with contributions from EC (16.3%), Cl^- (26%), NO_3^- (24.4%), Fe (22.9%), and Pb (60.2%). On the other hand, Factor 5, representing point source Fe contamination that enhances the dissolution of iron-rich minerals, contributes 11.4% of the total pollution to groundwater and is represented by HCO_3^- (24%), Mg^{2+} (18.7%), Pb (32%) and Fe (60.2%). Finally, unidentified sources contribute approximately 32% (Fig. 6a) of the total contribution of pollution to groundwater chemistry on average, represented by Temp (77.5%), pH (76%), HCO_3^- (44.6%), K^+ (25.1%), Cl^- (24%), NO_3^- (45.1%), and Ni (36.1%) based on the APCS-MLR receptor model (Fig. 6b).

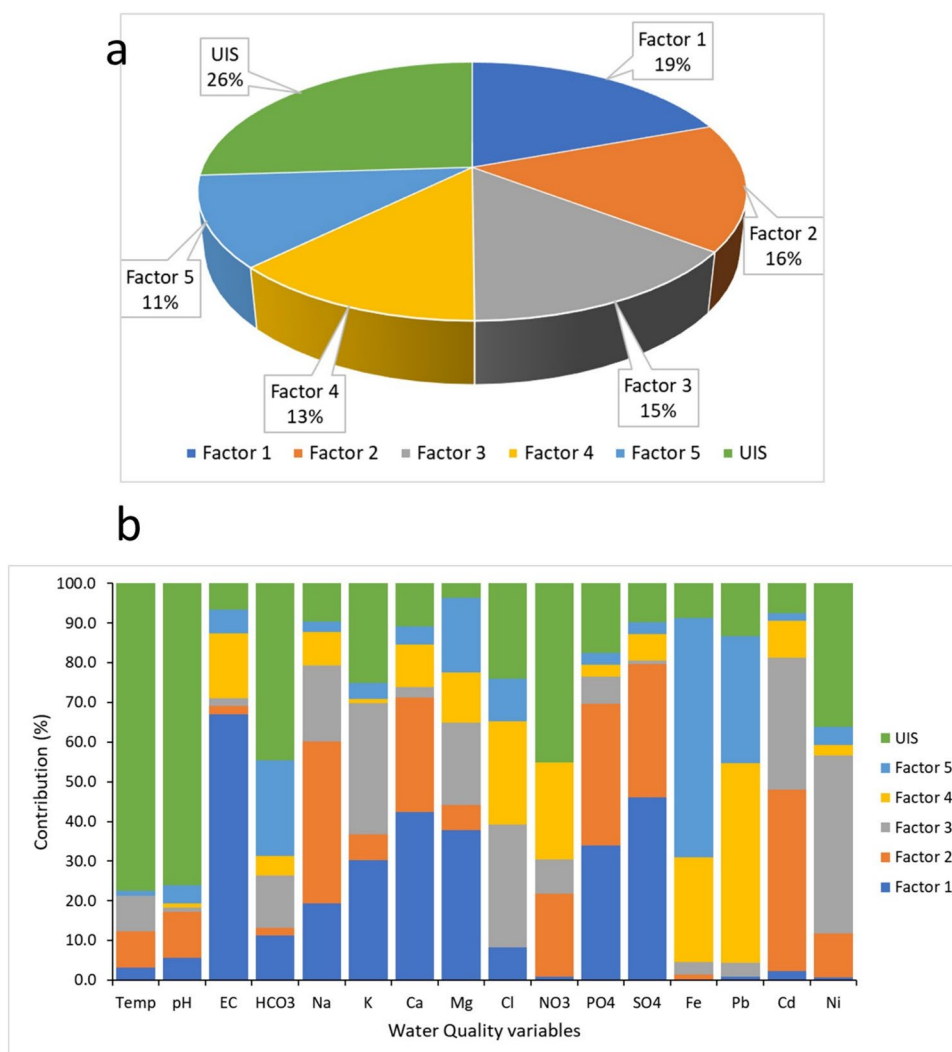
Table 10 Percentage pollution source apportionment based on the APCS-MLR receptor model

Parameters	Percentage pollution source contribution to the sampled groundwater					UIS	R^2	Adjusted R^2
	Factor 1	Factor 2	Factor 3	Factor 4	Factor 5			
Temp	3.19	9.04	9.01	0.06	1.25	77.45	0.55	0.46
pH	5.54	11.71	0.97	1.10	4.66	76.02	0.70	0.64
EC	67.00	2.03	1.99	16.30	6.07	6.61	0.98	0.97
HCO_3^-	11.32	1.84	13.20	4.98	24.04	44.62	0.96	0.95
Na^+	19.32	40.76	19.31	8.34	2.73	9.55	0.93	0.91
K^+	30.30	6.49	33.08	1.06	3.96	25.10	0.85	0.81
Ca^{2+}	42.30	28.87	2.69	10.79	4.44	10.91	0.84	0.80
Mg^{2+}	37.79	6.43	20.60	12.82	18.71	3.66	0.83	0.79
Cl^-	8.18	0.09	30.91	25.98	10.85	23.99	0.93	0.92
NO_3^-	0.92	20.83	8.71	24.40	0.07	45.07	0.67	0.59
PO_4^{3-}	34.01	35.55	6.95	3.01	2.93	17.55	0.88	0.85
SO_4^{2-}	45.99	33.63	0.88	6.69	3.04	9.77	0.93	0.91
Fe	0.22	1.24	3.12	26.45	60.21	8.76	0.88	0.85
Pb	0.79	0.11	3.41	50.43	31.95	13.31	0.84	0.80
Cd	2.33	45.60	33.38	9.20	2.03	7.47	0.78	0.73
Ni	0.75	11.00	44.83	2.65	4.68	36.09	0.56	0.47
Mean	19.4	16.0	14.6	12.8	11.4	26.0	0.8	0.8

UIS = unidentified sources

Values in bold indicate the most influential variables to each Factor

Fig. 6 Percentage contribution of pollution sources in the district; **a** average percentage contributions of sources; **b** percentage contributions of water quality parameters to pollution sources based on the APCS-MLR receptor model



5 Discussion

5.1 Mineralization process insight from hydrogeochemistry (water-rock interaction)

A clue to the dominant process that controls the chemistry of groundwater can be determined from a modified Gibbs plot of the ionic ratios of the major groundwater ions (Marandi and Shand 2018) (Fig. 7). The plotted data in the figure show that the groundwater system was primarily controlled by water-rock interaction. For a greater understanding of the process governing the interplay between water and rock, a plot of Na-normalized molar ratios of Ca^{2+} , Mg^{2+} , and HCO_3^- (Fig. 8) is mostly used on the scientific front (Halim et al. 2010). The groundwater data plotted in Fig. 8a and b indicate that silicate weathering and silicate mineral dissolution were the most likely primary water-rock interaction control of groundwater quality in the district.

In addition, the plot of $[\text{Ca}^{2+} + \text{Mg}^{2+}]$ vs. $[\text{SO}_4^{2-} + \text{HCO}_3^-]$ (Fig. 9a) might be used to deduce the likely mineral origins (silicate, carbonate, and/or gypsum) of the Ca^{2+} , Mg^{2+} , SO_4^{2-} , and HCO_3^- concentrations in the groundwater (Eyankware et al. 2020). Deduction from this graph, if borehole data plot below the 1:1 line, may indicate base cation exchange as a significant process affecting the groundwater chemistry, while data plotted above the 1:1 line may also indicate reverse cation exchange influences. About 11% of the data were plotted on the 1:1 line, suggesting a small fraction of carbonate minerals and to some extent dissolution of gypsum may have been one of the likely sources of the ion concentrations of Ca^{2+} , Mg^{2+} , SO_4^{2-} , and HCO_3^- in the sampled groundwater. Most groundwater samples (around 59% of the data plotted below the 1:1 line) are influenced by processes that include ion exchange and silicate weathering. A few of the groundwater samples (14%) from the plot suggest reverse ion exchange also influenced the groundwater.

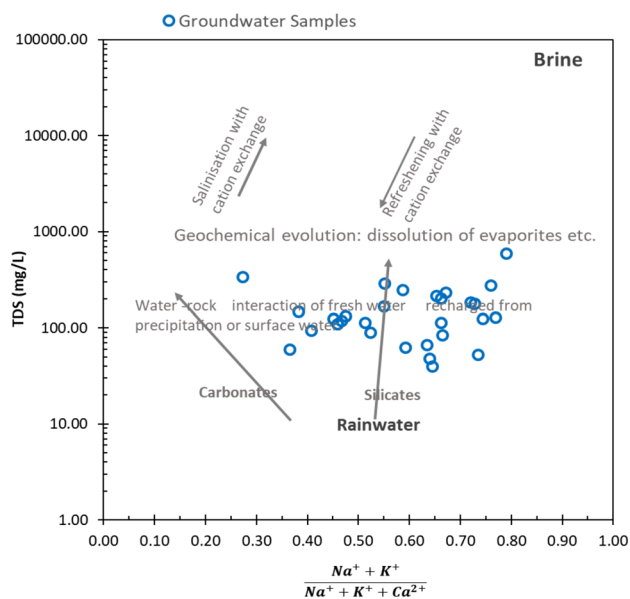


Fig. 7 Modified Gibbs plot after Marandi and Shand (2018) to show the main control of groundwater chemistry

Also, from the plot of $\text{Ca}^{2+}/\text{Mg}^{2+}$ vs. HCO_3^- , about 82.7% of the sampled Ca^{2+} , Mg^{2+} and HCO_3^- in groundwater may be sourced from silicate weathering (Fig. 9b), while about 7% and 10.3% of the sampled groundwater may have Ca^{2+} , Mg^{2+} and HCO_3^- sourced from calcite and dolomite, respectively.

The plot of $(\text{Ca}^{2+} + \text{Mg}^{2+}) - (\text{SO}_4^{2-} - \text{CO}_3^{2-})$ vs. $(\text{Na}^+ + \text{K}^+ - \text{Cl}^-)$ (Fig. 9c) was utilized to examine the ion exchange processes between the groundwater and its surrounding medium. A straight line ($R^2 = 0.9536$) with a slope

of -0.9357 was observed in the plot, indicating that ion exchange reactions were undergone by all sampled groundwater. Additionally, it was noted that the ion exchange process involved Na^+ , Ca^{2+} , and Mg^{2+} as the plot's y-intercept was almost at the origin.

To investigate the nature of the ion exchange processes, a plot of chloro-alkaline indices can be utilized (Osiakwan et al. 2021). The equations to compute CAI-I and CAI-II are provided as

$$\text{CAI-I} = \frac{\text{Cl}^- - (\text{Na}^+ + \text{K}^+)}{\text{Cl}^-} \quad (24)$$

$$\text{CAI-II} = \frac{\text{Cl}^- - (\text{Na}^+ + \text{K}^+)}{\text{HCO}_3^- + \text{SO}_4^{2-} + \text{NO}_3^-} \quad (25)$$

where all concentrations are in meq/L.

The plot in Fig. 9d shows that the base ion exchange region contained around 89.7% of the samples, indicating that the predominant nature of the ion exchange processes was base ion exchange. Nonetheless, a small percentage of the sampled data (about 10.3%) was noted to be plotted in the reverse ion exchange region.

The probable source for Na^+ , K^+ , Mg^{2+} , Ca^{2+} , and HCO_3^- resulting from the silicate weathering mechanism was inferred using the bivariate plots of HCO_3^- versus Na^+ , K^+ , Ca^{2+} , and Mg^{2+} (Fig. 10) complemented with weathering/dissolution prediction reactions (Table 11) (Walraevens et al. 2018). Plotting of data on the 1:1 and 1.18:0.82 lines of the plot of HCO_3^- vs. Na^+ (Fig. 10a) may indicate the weathering and incongruent dissolution of silicate minerals (albite and plagioclase). The plot of

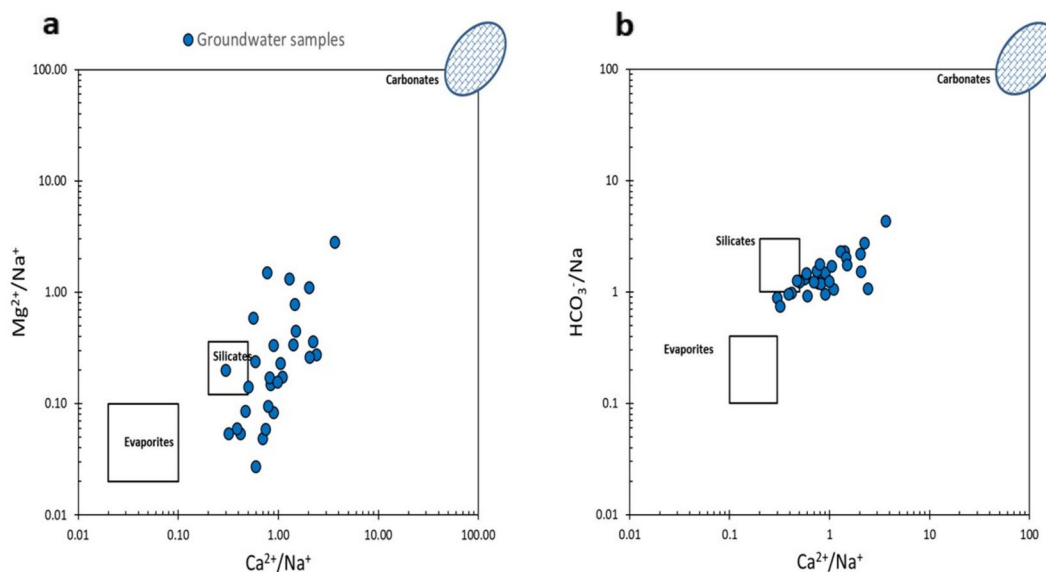
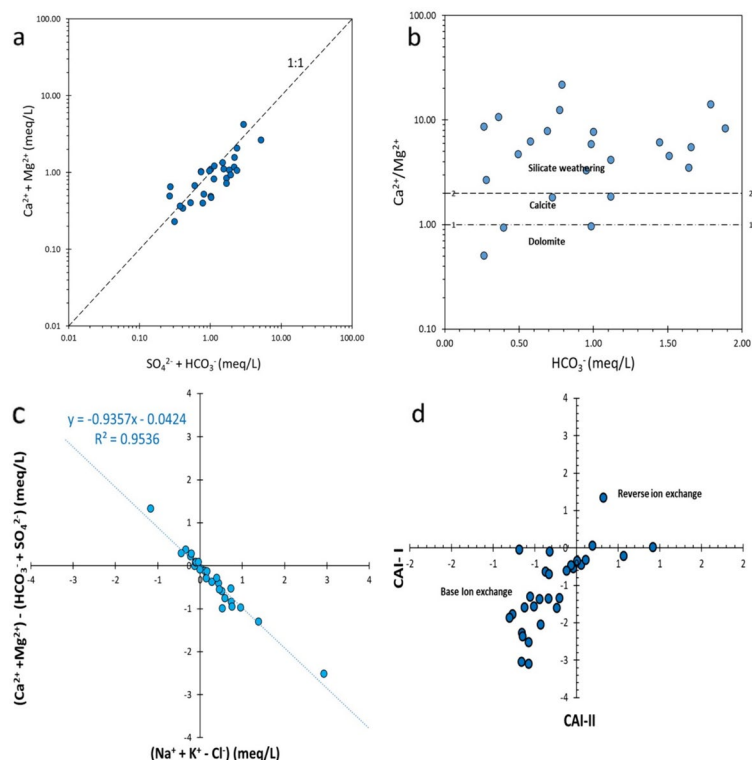


Fig. 8 A plot of **a** $\text{Mg}^{2+}/\text{Na}^+$ against $\text{Ca}^{2+}/\text{Na}^+$; **b** HCO_3^- against $\text{Ca}^{2+}/\text{Na}^+$

Fig. 9 A plot of **a** $[\text{Ca}^{2+} + \text{Mg}^{2+}]$ vs. $[\text{SO}_4^{2-} + \text{HCO}_3^-]$; **b** $\text{Ca}^{2+}/\text{Mg}^{2+}$ vs. HCO_3^- ; **c** $(\text{Ca}^{2+} + \text{Mg}^{2+}) - (\text{SO}_4^{2-} - \text{HCO}_3^-)$ vs. $(\text{Na}^+ + \text{K}^+ - \text{Cl}^-)$; **d** CAI-II against CAI-I



HCO_3^- versus Na^+ shows that approximately 38% may be influenced by the incongruent dissolution of albite and plagioclase (data points fell on 1:1 and 1.18:0.82 line) when considering the common rock types ($\text{NaAlSi}_3\text{O}_8$ and $\text{CaAl}_2\text{Si}_2\text{O}_8$) in the area. More than half of the groundwater sampled (about 62%) plotted above the 1:1 line, indicating excess HCO_3^- over Na^+ in groundwater.

Also, considering the plot of HCO_3^- versus Ca^{2+} (Fig. 10b), about 14% of the data points were plotted on and along the 1:1 line, implying perhaps the dissolution of calcite. About 62% of the data points were plotted on the 2:1 line, suggesting anorthite minerals may be contributing to the Ca^{2+} and HCO_3^- concentrations observed in the samples. About 24% of the data points are plotted below the 1:1 line, indicating other sources of Ca^{2+} in most of the groundwater samples.

However, on the HCO_3^- versus Mg^{2+} plot (Fig. 10c), about 4%, 7%, and 7% of groundwater data were plotted on the 5:8, 2:1, and 1.7:0.7 lines, respectively. This may suggest that the Mg^{2+} and HCO_3^- may be sourced from the biotite, dolomite, and pyroxene. The rest of the data points, thus, about 82%, plotted above the 1.7:0.7 line, indicating excess HCO_3^- over Mg^{2+} .

Lastly, on the plot of HCO_3^- versus K^+ (Fig. 10d), about 55.2% and 34.5% were plotted on the 5:2 line and 1:1 line, respectively. This indicates that the K^+ and HCO_3^- in the groundwater may be sourced from weathering of K-feldspar and biotite. Furthermore, 6.9% of the data were plotted

below the 1:1 line, indicating a K^+ excess over HCO_3^- , while only one sample (3.4% of the data) was plotted above the 5:2 line, indicating an HCO_3^- excess over K^+ .

5.2 Mineral saturation indices

Saturation indices (SI) are a useful measure to assess groundwater quality as they indicate the propensity of minerals to dissolve or precipitate in water (Appelo and Postma 1996). The statistical overview of the SI for some mineral phases in the groundwater is presented in Table 12. Notably, all the examined samples display undersaturation of anhydrite, gypsum, halite, and sylvite, with SI values spanning from -5.72 to -2.91 (with a mean of -4.44), -5.47 to -2.64 (with a mean of -4.17), -9.03 to -6.55 (with a mean of -8.00), and -8.57 to -6.82 (with a mean of -7.88), correspondingly. The negative values of SI for anhydrite, gypsum, halite, and sylvite across all samples demonstrate their undersaturation in the groundwater, suggesting that the water has low mineral concentration and the capacity to dissolve more minerals. In contrast, the saturation of aragonite, calcite, and dolomite in BH1 indicates a high concentration of these minerals in the groundwater, which could potentially result in the precipitation of these minerals in the water.

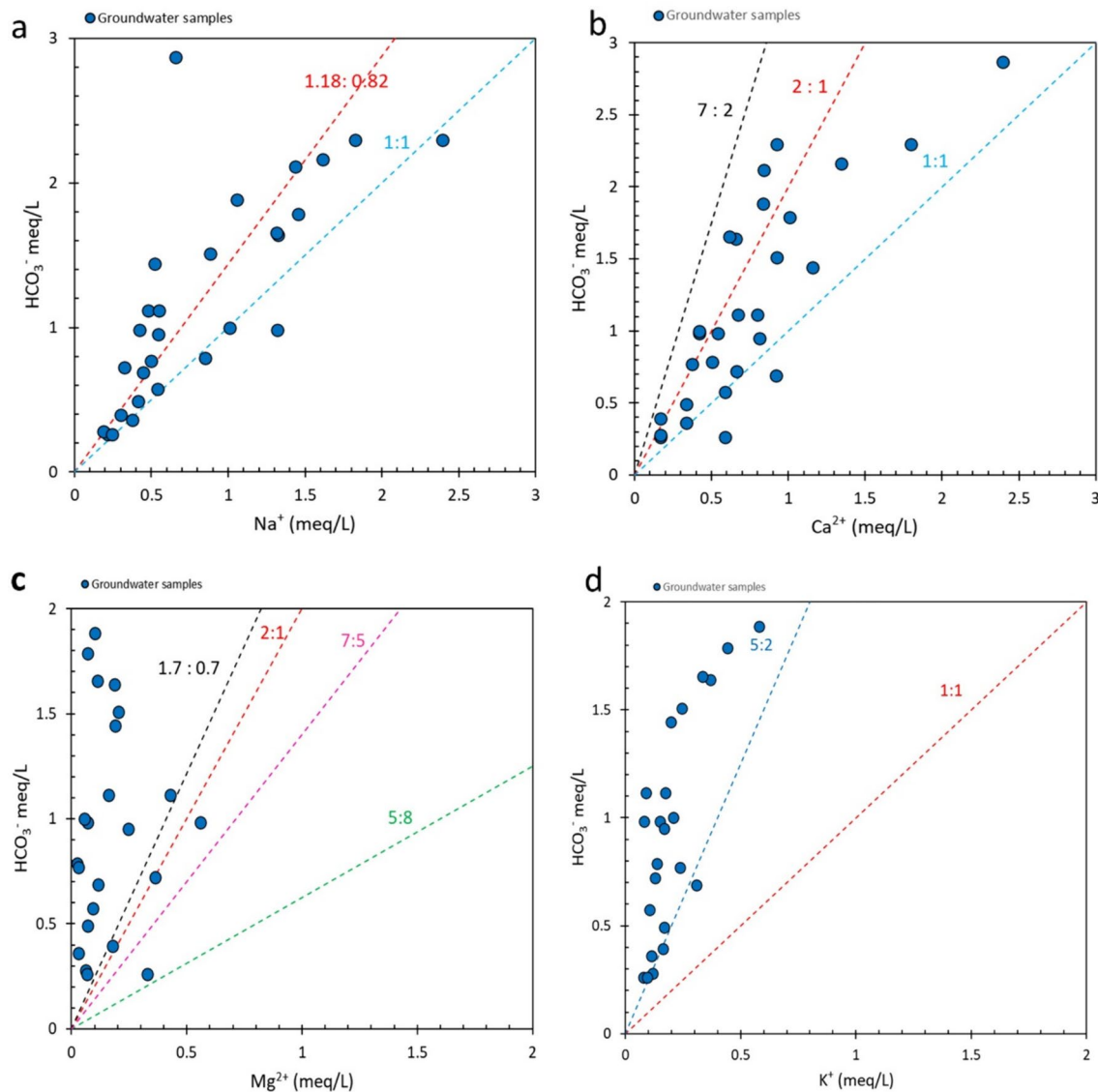


Fig. 10 A plot of HCO_3^- against **a** Na^+ ; **b** Ca^{2+} ; **c** Mg^{2+} ; **d** K^+ to identify probable source of major cations

5.3 Groundwater origin and origin of salinisation

The isotopic values in the area resulted in a lower correlation coefficient, possibly due to various factors like the local tropical climate, humidity, altitude, proximity to the sea, and wind direction. Figure 11a shows the sample points plotted closely around the global meteoric water line (GMWL), indicating the groundwater is of meteoric origin. Boreholes with a gradient of approximately 5.2, less than the GMWL, plotted below the regression line (evaporation line) as depicted in Fig. 11a.

Figure 11b shows the Cl^- versus $\delta^{18}\text{O}$ plot, which can be used to identify the mechanism of groundwater salinisation. The dissolution of minerals can be demonstrated on the plot when a considerable number of groundwater samples shows

similar $\delta^{18}\text{O}$ but increased chloride concentration (Gibrilla et al. 2010). Also, a high concentration of chloride found in groundwater samples may indicate contamination resulting from human activities like the discharge of wastewater from industrial facilities or septic systems. Based on the IEWQI classification, the plot of Cl^- versus $\delta^{18}\text{O}$ of groundwater samples revealed that groundwater with poor and extremely poor water quality had increased Cl^- concentration. This indicates mineral dissolution and significant pollution of groundwater from anthropogenic activities.

Table 11 Some common mineral weathering/dissolution prediction reactions

Reactions	Ratio
$\text{NaCl (Halite)} \rightarrow \text{Na}^+ + \text{Cl}^-$	$\text{Na}^+:\text{Cl}^- = 1:1$
$2\text{NaAlSi}_3\text{O}_8(\text{Albite}) + 9\text{H}_2\text{O} + 2\text{H}_2\text{CO}_3$ $\rightarrow \text{Al}_2\text{Si}_2\text{O}_5(\text{OH})_4 + 2\text{Na}^+ + 2\text{HCO}_3^- + 4\text{H}_4\text{SiO}_4$	$\text{Na}^+:\text{HCO}_3^- = 1:1$
$(\text{Na}_{0.82}\text{Ca}_{0.18})\text{Al}_{1.18}\text{Si}_{2.82}\text{O}_8(\text{Plagioclase}) + 1.18\text{CO}_2 + 1.77\text{H}_2\text{O}$ $\rightarrow 0.82\text{Na}^+ + 0.18\text{Ca}^{2+} + 1.18\text{HCO}_3^- + 0.59\text{Al}_2\text{Si}_2\text{O}_5(\text{OH})_4 + 1.64\text{SiO}_2$	$\text{Na}^+:\text{HCO}_3^- = 0.82:1.18$ $\text{Ca}^{2+}:\text{HCO}_3^- = 0.18:1.18$
$\text{CaCO}_3(\text{Calcite}) + \text{CO}_2 + \text{H}_2\text{O} \rightarrow \text{Ca}^{2+} + 2\text{HCO}_3^-$	$\text{Ca}^{2+}:\text{HCO}_3^- = 1:2$
$2\text{CaAl}_2\text{Si}_3\text{O}_8(\text{Anorthite}) + 4\text{CO}_2 + 6\text{H}_2\text{O} \rightarrow 2\text{Al}_2\text{Si}_2\text{O}_5(\text{OH})_4 + 2\text{Ca}^{2+} + 4\text{HCO}_3^-$	$\text{Ca}^{2+}:\text{HCO}_3^- = 1:2$
$\text{CaSO}_4(\text{Gypsum}) \rightarrow \text{Ca}^{2+} + \text{SO}_4^{2-}$	$\text{Ca}^{2+}:\text{SO}_4^{2-} = 1:1$
$\text{CaMg}(\text{CO}_3)_2(\text{Dolomite}) + 2\text{CO}_2 + 2\text{H}_2\text{O} \rightarrow \text{Ca}^{2+} + \text{Mg}^{2+} + 4\text{HCO}_3^-$	$\text{Ca}^{2+}:\text{Mg}^{2+} = 1:1$ $\text{Ca}^{2+}:\text{HCO}_3^- = 1:4$
$\text{Ca}_2\text{Mg}_5\text{Si}_2\text{O}_{22}(\text{OH})_2(\text{Amphibole}) + 14\text{CO}_2 + 22\text{H}_2\text{O}$ $\rightarrow 2\text{Ca}^{2+} + 5\text{Mg}^{2+} + 14\text{HCO}_3^- + 8\text{H}_4\text{SiO}_4$	$\text{Ca}^{2+}:\text{HCO}_3^- = 1:7$ $\text{Mg}^{2+}:\text{HCO}_3^- = 2.5:7$
$\text{CaMg}_{0.7}\text{Fe}_{0.3}\text{Si}_2\text{O}_6(\text{Pyroxene}) + 3.4\text{CO}_2 + 2.3\text{H}_2\text{O}$ $\rightarrow \text{Ca}^{2+} + 0.7\text{Mg}^{2+} + 2\text{SiO}_2 + 3.4\text{HCO}_3^- + 0.3\text{H}^+ + 0.3\text{Fe}(\text{OH})_3$	$\text{Ca}^{2+}:\text{HCO}_3^- = 1:3.4$ $\text{Mg}^{2+}:\text{HCO}_3^- = 0.7:3.4$
$2\text{K}(\text{Mg}_2\text{Fe})(\text{AlSi}_3)\text{O}_{10}(\text{OH})_2(\text{Biotite}) + 5\text{H}_2\text{CO}_3 + 7\text{H}_2\text{CO}_3 + 7\text{H}_2\text{O}$ $\rightarrow \text{Al}_2\text{Si}_2\text{O}_5(\text{OH})_4 + 2\text{K}^+ + 4\text{Mg}^{2+} + 2\text{Fe}(\text{OH})_3 + 4\text{H}_4\text{SiO}_4 + 5\text{HCO}_3^-$	$\text{Mg}^{2+}:\text{HCO}_3^- = 4:5$ $\text{K}^+:\text{HCO}_3^- = 2:5$
$2\text{KAlSi}_3\text{O}_8(\text{K-feldspar}) + 9\text{H}_2\text{O} + 2\text{H}_2\text{CO}_3$ $\rightarrow \text{Al}_2\text{Si}_2\text{O}_5(\text{OH})_4 + 2\text{K}^+ + 2\text{HCO}_3^- + 4\text{H}_4\text{SiO}_4$	$\text{K}^+:\text{HCO}_3^- = 1:1$

5.4 Study limitations and future directions

The study, while providing valuable insights, has a few limitations. The sample size of 29 groundwater points, though providing a good overview, may not fully capture all hydro-geochemical variations across the entire basin; hence, the spatial distribution was constrained by accessible boreholes, potentially underrepresenting certain areas. Additionally,

Table 12 Summary statistics of saturation indices calculations using PHREEQC

Mineral saturation indices	Minimum	Maximum	Mean
Anhydrite	-5.72	-2.91	-4.44
Aragonite	-3.47	0.36	-1.30
Calcite	-3.32	0.51	-1.15
CO ₂ (g)	-3.37	-1.33	-2.27
Dolomite	-6.92	1.06	-2.78
Fe(OH) ₃ (a)	-3.85	0.39	-1.98
Goethite	1.90	6.43	4.03
Gypsum	-5.47	-2.64	-4.17
Halite	-9.03	-6.55	-8.00
Melanterite	-9.32	-7.35	-8.49
Otavite	-3.41	1.23	-1.55
Pb(OH) ₂	-4.44	-0.82	-2.45
Siderite	-2.03	1.01	-0.66
Sylvite	-8.57	-6.82	-7.88
Cerussite	-3.16	-0.25	-1.73

this study represents a snapshot from January 2019, not accounting for potential seasonal variations in groundwater chemistry and stable isotopes. Lastly, the study did not analyse stable isotopes of surface water, which hindered a detailed analysis of surface water-groundwater interactions.

To overcome these limitations and build on the findings, several directions for future research are proposed. An expanded sampling programme should aim to increase both the number and spatial distribution of sampling points, potentially including the installation of additional monitoring wells in underrepresented areas. Implementing a long-term monitoring programme with seasonal sampling would allow the assessment of temporal variations and the identification of long-term trends. Where possible, future studies should incorporate depth-specific sampling to better understand the three-dimensional nature of the aquifer system. More extensive use of environmental isotopes (surface water and rainwater) could provide additional insights into groundwater age, recharge processes, surface water-groundwater interactions, and flow patterns.

6 Conclusion

The application of ionic ratio graphs, multivariate statistics (PCA for the major factors influencing groundwater quality and APCS-MRL receptor model for source apportionment), geochemical modelling, stable isotopes of $\delta^2\text{H}$ and $\delta^{18}\text{O}$, and geostatistics techniques has provided significant insights into

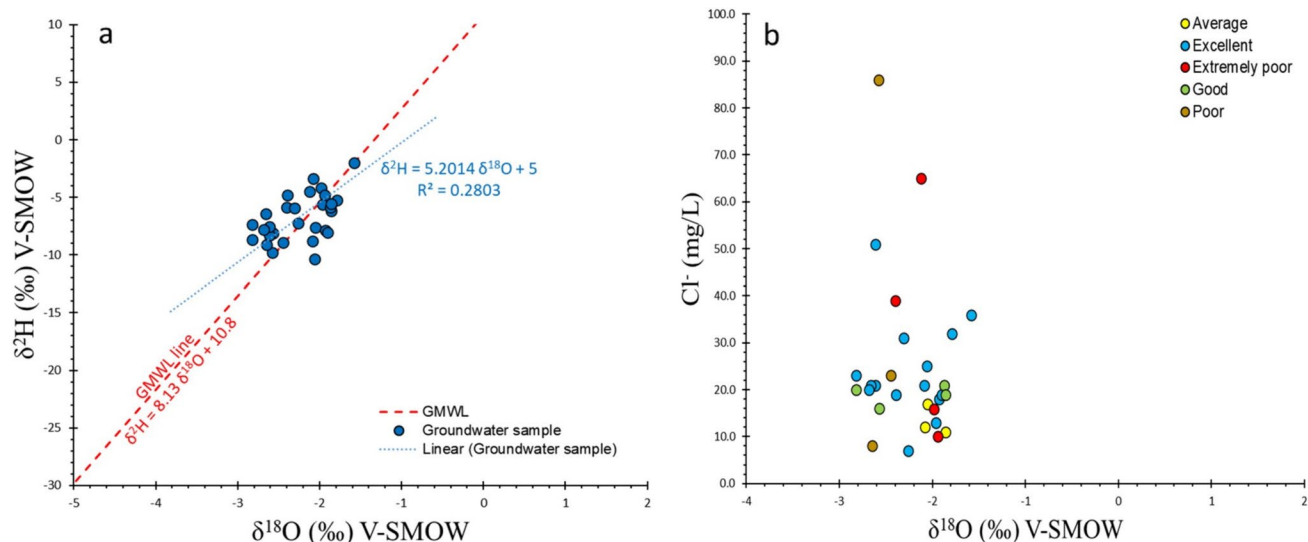


Fig. 11 A plot of **a** $\delta^2\text{H}$ against $\delta^{18}\text{O}$ to show the origin of groundwater; **b** Cl^- against $\delta^{18}\text{O}$ to show the mechanism of groundwater quality

the groundwater origin and quality in the Wassa District in the Lower Pra Basin, Ghana, using 29 groundwater samples. The outcome of the study highlights that:

- The average trend of cation dominance was $\text{Na}^+ > \text{Ca}^{2+} > \text{K}^+ > \text{Mg}^{2+}$, while the average trend of anion dominance was $\text{HCO}_3^- > \text{Cl}^- > \text{SO}_4^{2-} > \text{NO}_3^- > \text{PO}_4^{3-}$; also the trend of trace element dominance was in the order $\text{Pb} > \text{Fe} > \text{Ni} > \text{Cd}$ in the groundwater sampled.
- The hydrochemical facies observed are $\text{Ca-Mg-HCO}_3\text{-Cl}$, Ca-Na-HCO_3 , Na-Ca-HCO_3 , $\text{Ca-Na-HCO}_3\text{-Cl}$, $\text{Na-Ca-HCO}_3\text{-Cl}$, mix water type, and $\text{Na-HCO}_3\text{-Cl}$, and all evolved to Ca-Na-Cl-HCO_3 , and Na-Ca-Cl-HCO_3 .
- About 53.6%, 14.3%, 14.3%, 7.1%, and 10.7% of the groundwater samples were classified as excellent, good, average, poor, and extremely poor quality, respectively, according to the IEWQI for drinking. For irrigation purposes, based on the IWQI, about 3.45% are safe to use for irrigation without any treatment. About 41.4% are relatively safe to use for irrigation, but some treatment may be necessary. About 37.9%, 13.8%, and 3.45% were classified as a moderate, high, and severe restriction zones for irrigation water.
- The main control of groundwater chemistry was water-rock interaction, largely silicate weathering and dissolution of minerals (K-feldspar, albite, and plagioclase and to some extent biotite, dolomite, calcite, and pyroxene), cation base exchange processes, and anthropogenic activities like mining and quarrying.
- PCA results suggest that groundwater chemistry is affected by a combination of natural and anthropogenic sources.
- Based on the APCS-MLR receptor model, the multiple influences on the groundwater chemistry were quantified as mineral dissolution and weathering, contributing significantly to salinisation with approximately 16.2%, followed by trace metal contamination (primarily Cd) from industrial activities at 16%. Nickel contamination (Ni and K^+) from mineral weathering and urban activities contributes around 13.4%, while industrial activities such as quarrying account for 12.1%. Dissolution of iron-rich minerals and unidentified sources make up 10.3% and 32% of the influence on groundwater chemistry, respectively.
- Based on aqueous speciation modelling, the examined groundwater samples, except for one sample (BH1), showed undersaturation of aragonite, calcite, dolomite anhydrite, gypsum, halite, and sylvite, indicating low mineral concentration and the ability to dissolve more minerals.
- The origin of groundwater in the district was meteoric and indicates direct infiltration. Furthermore, the plots of Cl^- versus $\delta^{18}\text{O}$ provide insights into the mechanism of groundwater salinisation, suggesting the dissolution of minerals and significant pollution from anthropogenic activities.

Acknowledgements The successful completion of this scientific manuscript was made possible by the contributions of many individuals, and we would like to extend our heartfelt gratitude to them. Specifically, we extend our gratitude to the GAEC isotope laboratory staff, whose valuable assistance in analysing the stable isotopes ($\delta^2\text{H}$ and $\delta^{18}\text{O}$). The chemistry laboratory staff also deserves recognition for their technical support and meticulous attention to detail in analysing the water samples, which helped ensure the quality of our data. We

are deeply grateful for the contributions of all individuals involved in reviewing this research paper, as their efforts have significantly improved the paper.

Author contributions Samuel Y. Ganyaglo: conceptualization, formal analysis, methodology, visualization, editing; Joel Y Binyiako: conceptualization, formal analysis, methodology, visualization, writing-original draft preparation; Emmanuel M Teye: writing-reviewing and editing; Abass Gibrilla: investigation, data curation, writing-reviewing and editing; Dickson Abdul-Wahab: writing-reviewing and editing; Samuel Edusei: writing-reviewing and editing; Paulina Amponsah: supervision, writing-reviewing and editing; Courage D Egbi: writing-reviewing and editing; Samuel B Dampare: supervision, writing-reviewing and editing; Ebenezer Aquisman Asare: writing-reviewing and editing.

Data availability Data sets generated during the current study are available from the corresponding author on reasonable request.

Declarations

Conflict of interest The authors declare that they have no known competing financial interests or personal relationships that could have appeared to influence the work reported in this paper.

Consent to participate All the authors have consented to participate in the publication.

Consent for publication All authors agreed on the content and publication of the manuscript.

References

- Abanyie SK, Sunkari ED, Apea OB, Abagale S, Korboe HM (2020) Assessment of the quality of water resources in the Upper East Region, Ghana: a review. *Sustain Water Resour Manag* 6(4):1–18. <https://doi.org/10.1007/s40899-020-00409-4>
- Abbasi T, Abbasi S (2012) Water quality indices. In: Water quality indices. Elsevier. <https://doi.org/10.1016/C2010-0-69472-7>
- Abbasnia A, Yousefi N, Mahvi AH, Nabizadeh R, Radfard M, Yousefi M, Alimohammadi M (2019) Evaluation of groundwater quality using water quality index and its suitability for assessing water for drinking and irrigation purposes: case study of Sistan and Baluchistan province (Iran). *Hum Ecol Risk Assess* 25(4):988–1005. <https://doi.org/10.1080/10807039.2018.1458596>
- Abdul-Wahab D, Gibrilla A, Adomako D, Adotey DK, Ganyaglo S, Laar C, Zakaria N, Anornu G (2022) Application of geostatistical techniques to assess groundwater quality in the Lower Anayari catchment in Ghana. *HydroResearch* 5:35–47. <https://doi.org/10.1016/j.hydres.2022.04.001>
- Abouchami W, Boher M, Michard A, Albarede F (1990) A major 2.1 Ga event of mafic magmatism in west Africa: an Early stage of crustal accretion. *J Geophys Res* 95(B11):17605. <https://doi.org/10.1029/JB095iB11p17605>
- Adomako D, Gibrilla A, Maloszewski P, Ganyaglo SY, Rai SP (2015) Tracing stable isotopes ($\delta^2\text{H}$ and $\delta^{18}\text{O}$) from meteoric water to groundwater in the Densu River basin of Ghana. *Environ Monit Assess* 187(5):264. <https://doi.org/10.1007/s10661-015-4498-2>
- Anornu G, Gibrilla A, Adomako D (2017) Tracking nitrate sources in groundwater and associated health risk for rural communities in the White Volta River basin of Ghana using isotopic approach ($\delta^{15}\text{N}$, $\delta^{18}\text{O}$ [sbnd] NO_3 and ^3H). *Sci Total Environ* 603–604:687–698. <https://doi.org/10.1016/j.scitotenv.2017.01.219>
- Appelo CAJ, Postma D (1996) Minerals and water. In: Balkema AA (ed) *Geochemistry, groundwater and pollution*, 2nd edn. CRC Press, London, pp 119–171.
- Argamasilla M, Barberá JA, Andreo B (2017) Factors controlling groundwater salinization and hydrogeochemical processes in coastal aquifers from southern Spain. *Sci Total Environ* 580:50–68. <https://doi.org/10.1016/j.scitotenv.2016.11.173>
- Armah YS (2010) Hydrochemical analysis of groundwater in the lower Pra basin of Ghana. *J Water Resour Prot* 02(10):864–871. <https://doi.org/10.4236/jwarp.2010.210103>
- Armah YS, Ahialey EK, Serfoh-Armah Y, Kortatsi BK (2010) Hydrochemical analysis of groundwater in the lower Pra basin of Ghana. *J Water Resour Prot* 2(10):864–871. <https://doi.org/10.4236/jwarp.2010.210103>
- Asare EA, Klutse CK, Opare-Boafo MS (2022) Assessment of groundwater quality, source distribution of fluoride and nitrate, and associate human health risk in a community in North-Eastern Ghana, Bolgatanga. *Chem Afr* 5(1):173–188. <https://doi.org/10.1007/s42250-021-00290-4>
- Banoeng-Yakubo B, Yidana SM, Anku Y, Akabzaa T, Asiedu D (2009) Water quality characterization in some Birimian aquifers of the Birim Basin, Ghana. *KSCE J Civ Eng* 13(3):179–187. <https://doi.org/10.1007/s12205-009-0179-4>
- Bari JA, Vennila G, Karthikeyan P (2021) Appraisal of hydrogeochemical processes and groundwater quality in Bhavani taluk Erode district, Tamil Nadu, India. *Arab J Geosci* 14(13):1228. <https://doi.org/10.1007/s12517-021-07516-2>
- Biddau R, Cidu R, Da Pelo S, Carletti A, Ghiglieri G, Pittalis D (2019) Source and fate of nitrate in contaminated groundwater systems: assessing spatial and temporal variations by hydrogeochemistry and multiple stable isotope tools. *Sci Total Environ* 647:1121–1136. <https://doi.org/10.1016/j.scitotenv.2018.08.007>
- Carasek FL, Baldissera R, Oliveira JV, Scheibe LF, Magro JD (2020) Quality of the groundwater of the Serra Geral Aquifer System of Santa Catarina west region, Brazil. *Groundw Sustain Dev* 10:100346. <https://doi.org/10.1016/j.gsd.2020.100346>
- Carrier M, Lefebvre R, Racicot J, Asare E (2008) Northern Ghana hydrogeological assessment project. In: Access to sanitation and safe water: global partnerships and local actions—proceedings of the 33rd WEDC international conference.
- Comte JC, Cassidy R, Obando J, Robins N, Ibrahim K, Melchioly S, Mjemah I, Shauri H, Bourhane A, Mohamed I, Noe C, Mwega B, Makokha M, Join JL, Banton O, Davies J (2016) Challenges in groundwater resource management in coastal aquifers of East Africa: investigations and lessons learnt in the Comoros Islands, Kenya and Tanzania. *J Hydrol Reg Stud* 5:179–199. <https://doi.org/10.1016/j.ejrh.2015.12.065>
- Dong H, Gao Z (2022) Theoretical progress of groundwater chemical evolution based on Tóthian theory: a review. *Front Mar Sci* 9(August):1–15. <https://doi.org/10.3389/fmars.2022.972426>
- Dorleku MK, Nukpezah D, Carboo D (2018) Effects of small-scale gold mining on heavy metal levels in groundwater in the Lower Pra Basin of Ghana. *Appl Water Sci* 8(5):126. <https://doi.org/10.1007/s13201-018-0773-z>
- Dorleku MK, Affum AO, Tay CK, Nukpezah D (2019) Assessment of Nutrients Levels in Groundwater within the Lower Pra Basin of Ghana. *Ghana J Sci* 60(1):24–36. <https://doi.org/10.4314/gjs.v60i1.3>
- Elumalai V, Rajmohan N, Sithole B, Li P, Uthandi S, van Tol J (2023) Geochemical evolution and the processes controlling groundwater chemistry using ionic ratios, geochemical modelling and

- chemometric analysis in uMhlathuze catchment, KwaZulu-Natal, South Africa. *Chemosphere* 312(P1):137179. <https://doi.org/10.1016/j.chemosphere.2022.137179>
- Enemark T, Peeters LJM, Mallants D, Batelaan O (2019) Hydrogeological conceptual model building and testing: a review. *J Hydrol* 569:310–329. <https://doi.org/10.1016/j.jhydrol.2018.12.007>
- Eyankware MO, Aleke CG, Selema AOI, Nnabo PN (2020) Hydrogeochemical studies and suitability assessment of groundwater quality for irrigation at Warri and environs, Niger delta basin, Nigeria. *Groundw Sustain Dev* 10:100293. <https://doi.org/10.1016/j.gsd.2019.100293>
- Farid I, Trabelsi R, Zouari K, Beji R (2013) Geochemical and isotopic study of surface and groundwaters in Ain Bou Mourra basin, central Tunisia. *Quat Int* 303:210–227. <https://doi.org/10.1016/j.quaint.2013.04.021>
- Gholizadeh HM, Melesse AM, Reddi L (2016) Water quality assessment and apportionment of pollution sources using APCS-MLR and PMF receptor modeling techniques in three major rivers of South Florida. *Sci Total Environ* 566–567:1552–1567. <https://doi.org/10.1016/j.scitotenv.2016.06.046>
- Gibrilla A, Osae S, Akiti TT, Adomako D, Ganyaglo SY, Bam EPK, Hadisu A (2010) Origin of dissolve ions in groundwaters in the Northern Densu River Basin of Ghana using stable isotopes of ^{18}O and ^2H . *J Water Resour Prot* 02(12):1010–1019. <https://doi.org/10.4236/jwarp.2010.212121>
- Gibrilla A, Adomako D, Anornu G, Ganyaglo S, Stigter T, Fianko JR, Rai S, Ako AA (2017) $\delta^{18}\text{O}$ and $\delta^2\text{H}$ characteristics of rainwater, groundwater and springs in a mountainous region of Ghana: implication with respect to groundwater recharge and circulation. *Sustain Water Resour Manag* 3(4):413–429. <https://doi.org/10.1007/s40899-017-0107-6>
- Gibrilla A, Fianko JR, Ganyaglo S, Adomako D, Stigter TY, Salifu M, Anornu G, Zango MS, Zakaria N (2022) Understanding recharge mechanisms and surface water contribution to groundwater in granitic aquifers, Ghana: insights from stable isotopes of $\delta^2\text{H}$ and $\delta^{18}\text{O}$. *J Afr Earth Sc* 192:104567. <https://doi.org/10.1016/j.jafrearsci.2022.104567>
- Gribov A, Krivoruchko K (2020) Empirical Bayesian kriging implementation and usage. *Sci Total Environ* 722:137290. <https://doi.org/10.1016/j.scitotenv.2020.137290>
- Halim MA, Majumder RK, Nessa SA, Hiroshiro Y, Sasaki K, Saha BB, Saepuloh A, Jinno K (2010) Evaluation of processes controlling the geochemical constituents in deep groundwater in Bangladesh: spatial variability on arsenic and boron enrichment. *J Hazard Mater* 180(1–3):50–62. <https://doi.org/10.1016/j.jhazmat.2010.01.008>
- Hameed M, Moradkhani H, Ahmadalipour A, Mofstakhari H, Abbaszadeh P, Alipour A (2019) A review of the 21st century challenges in the food–energy–water security in the middle east. *Water (Switzerland)* 11(4):682. <https://doi.org/10.3390/w11040682>
- Hooshmand A, Delghandi M, Izadi A, Aali KA (2011) Application of kriging and cokriging in spatial estimation of groundwater quality parameters. *Afr J Agric Res* 6(14):3402–3408. <https://doi.org/10.5897/AJAR11.027>
- Iqbal AB, Rahman MM, Mondal DR, Khandaker NR, Khan HM, Ahsan GU, Jakariya M, Hossain MM (2020) Assessment of Bangladesh groundwater for drinking and irrigation using weighted overlay analysis. *Groundw Sustain Dev* 10:100312. <https://doi.org/10.1016/j.gsd.2019.100312>
- ISARM-AFRICA. (2004). Shared aquifer resources in Africa. In UNESCO-IHP/ISARM international workshop-managing shared aquifer resources in Africa. IHP-VI, Series on Groundwater No. 8, vol 8.
- Jasechko S (2019) Global isotope hydrogeology—review. *Rev Geophys* 57(3):835–965. <https://doi.org/10.1029/2018RG000627>
- Jasrotia AS, Taloor AK, Andotra U, Kumar R (2019) Monitoring and assessment of groundwater quality and its suitability for domestic and agricultural use in the Cenozoic rocks of Jammu Himalaya, India: a geospatial technology based approach. *Groundw Sustain Dev* 8:554–566. <https://doi.org/10.1016/j.gsd.2019.02.003>
- Kaiser HF (1991) Coefficient alpha for a principal component and the Kaiser-Guttman rule. *Psychol Rep* 68(3):855–858.
- Kesse GO, Aukrah PT, Sharp WE (1992) Summary of Lake Bosumtwi water level-1932 to 1977. In Ghana Geological Survey Department, Accra, Report of the Director of Geological Survey for the Period, vol 1. pp 56–64.
- Khatri N, Tyagi S, Rawtani D, Tharmavaram M, Kamboj RD (2020) Analysis and assessment of ground water quality in Satlasana Taluka, Mehsana district, Gujarat, India through application of water quality indices. *Groundw Sustain Dev* 10(13):100321. <https://doi.org/10.1016/j.gsd.2019.100321>
- Loh YSA, Akurugu BA, Manu E, Aliou AS (2020) Assessment of groundwater quality and the main controls on its hydrochemistry in some Voltaian and basement aquifers, northern Ghana. *Groundw Sustain Dev* 10:100296. <https://doi.org/10.1016/j.gsd.2019.100296>
- Marandi A, Shand P (2018) Groundwater chemistry and the Gibbs diagram. *Appl Geochem* 97:209–212. <https://doi.org/10.1016/j.apgeochem.2018.07.009>
- Meireles ACM, de Andrade EM, Chaves LCG, Frischkorn H, Crisostomo LA (2010) A new proposal of the classification of irrigation water. *Revista Ciência Agronômica* 41(3):349–357. <https://doi.org/10.1590/s1806-66902010000300005>
- Meng L, Zuo R, Wang JS, Yang J, Teng YG, Shi RT, Zhai YZ (2018) Apportionment and evolution of pollution sources in a typical riverside groundwater resource area using PCA-APCS-MLR model. *J Contam Hydrol* 218(April):70–83. <https://doi.org/10.1016/j.jconhyd.2018.10.005>
- Mohanty AK, Lingaswamy M, Rao VG, Sankaran S (2018) Impact of acid mine drainage and hydrogeochemical studies in a part of Rajrappa coal mining area of Ramgarh District, Jharkhand State of India. *Groundw Sustain Dev* 7:164–175. <https://doi.org/10.1016/j.gsd.2018.05.005>
- Mthembu PP, Elumalai V, Brindha K, Li P (2020) Hydrogeochemical processes and trace metal contamination in groundwater: impact on human health in the maputaland coastal aquifer, South Africa. *Expo Health* 12(3):403–426. <https://doi.org/10.1007/s12403-020-00369-2>
- Omre H (1987) Bayesian kriging—merging observations and qualified guesses in kriging. *Math Geol* 19(1):25–39. <https://doi.org/10.1007/BF01275432>
- Osiakwan GM, Appiah-Adjei EK, Kabo-Bah AT, Gibrilla A, Anornu G (2021) Assessment of groundwater quality and the controlling factors in coastal aquifers of Ghana: an integrated statistical, geostatistical and hydrogeochemical approach. *J Afr Earth Sc* 184(April):104371. <https://doi.org/10.1016/j.jafrearsci.2021.104371>
- Pei-Yue L, Qian H, Jian-Hua W (2010) Groundwater quality assessment based on improved water quality index in Pengyang County, Ningxia, Northwest China. *E-J Chem* 7(S1):S209–S216.
- Pei-Yue L, Hui Q, Jian-Hua W (2011) Application of set pair analysis method based on entropy weight in groundwater quality assessment—a case study in Dongsheng City, Northwest China. *E-J Chem* 8(2):851–858. <https://doi.org/10.1155/2011/879683>
- Purushotham D, Rashid M, Lone MA, Rao AN, Ahmed S, Nagaiah E, Dar FA (2013) Environmental impact assessment of air and heavy metal concentration in groundwater of Maheshwaram watershed, Ranga Reddy district, Andhra Pradesh. *J Geol Soc India* 81(3):385–396. <https://doi.org/10.1007/s12594-013-0049-z>
- Ram A, Tiwari SK, Pandey HK, Chaurasia AK, Singh S, Singh YV (2021) Groundwater quality assessment using water quality index

- (WQI) under GIS framework. *Appl Water Sci* 11(2):46. <https://doi.org/10.1007/s13201-021-01376-7>
- Samsonova VP, Blagoveshchenskii YN, Meshalkina YL (2017) Use of empirical Bayesian kriging for revealing heterogeneities in the distribution of organic carbon on agricultural lands. *Eurasian Soil Sci* 50(3):305–311. <https://doi.org/10.1134/S1064229317030103>
- Scanlon BR, Reedy RC, Stonestrom DA, Prudic DE, Dennehy KF (2005) Impact of land use and land cover change on groundwater recharge and quality in the southwestern US. *Glob Change Biol* 11(10):1577–1593. <https://doi.org/10.1111/j.1365-2486.2005.01026.x>
- Shelton JL, Engle MA, Bucciatti A, Blondes MS (2018) The isometric log-ratio (ilr)-ion plot: a proposed alternative to the Piper diagram. *J Geochem Explor* 190(February):130–141. <https://doi.org/10.1016/j.gexplo.2018.03.003>
- Snousy MG, Morsi MS, Elewa AMT, Ahmed SAE, El-Sayed E (2020) Groundwater vulnerability and trace element dispersion in the Quaternary aquifers along middle Upper Egypt. *Environ Monit Assess* 192(3):174. <https://doi.org/10.1007/s10661-020-8109-5>
- Spalding RFF, Hirsh AJJ, Exner MEE, Little NAA, Kloppenborg KLL (2019) Applicability of the dual isotopes $\delta^{15}\text{N}$ and $\delta^{18}\text{O}$ to identify nitrate in groundwater beneath irrigated cropland. *J Contam Hydrol* 220:128–135. <https://doi.org/10.1016/j.jconhyd.2018.12.004>
- Su J, Qiu Y, Lu Y, Yang X, Li S (2021) Use of multivariate statistical techniques to study spatial variability and sources apportionment of pollution in rivers flowing into the Laizhou Bay in Dongying District. *Water* 13(6):772. <https://doi.org/10.3390/w13060772>
- Sunkari ED, Abu M, Zango MS (2021) Geochemical evolution and tracing of groundwater salinization using different ionic ratios, multivariate statistical and geochemical modeling approaches in a typical semi-arid basin. *J Contam Hydrol* 236:103742. <https://doi.org/10.1016/j.jconhyd.2020.103742>
- Walraevens K, Bakundukize C, Mtoni YE, Van Camp M (2018) Understanding the hydrogeochemical evolution of groundwater in Precambrian basement aquifers: a case study of Bugesera region in Burundi. *J Geochem Explor* 188:24–42. <https://doi.org/10.1016/j.gexplo.2018.01.003>
- Werner AD, Bakker M, Post VEA, Vandenbohede A, Lu C, Ataie-Ashtiani B, Simmons CT, Barry DA (2013) Seawater intrusion processes, investigation and management: recent advances and future challenges. *Adv Water Resour* 51:3–26. <https://doi.org/10.1016/j.advwatres.2012.03.004>
- WHO/UNICEF (2019) Drinking-water. Newsroom.
- World Health Organization (WHO) (2011) Guidelines for drinking-water quality. In World Health Organization 2011. WHO Press, World Health Organization.
- Yidana SM, Banoeng-Yakubo B, Sakyi PA (2012) Identifying key processes in the hydrochemistry of a basin through the combined use of factor and regression models. *J Earth Syst Sci* 121(2):491–507.
- Yu L, Zheng T, Yuan R, Zheng X (2022) APCS-MLR model: a convenient and fast method for quantitative identification of nitrate pollution sources in groundwater. *J Environ Manag* 314:115101. <https://doi.org/10.1016/j.jenvman.2022.115101>
- Springer Nature or its licensor (e.g. a society or other partner) holds exclusive rights to this article under a publishing agreement with the author(s) or other rightsholder(s); author self-archiving of the accepted manuscript version of this article is solely governed by the terms of such publishing agreement and applicable law.